UNIVERSIDADE DE LISBOA
FACULDADE DE CIÊNCIAS
DEPARTAMENTO DE BIOLOGIA ANIMAL

Decellularized fetal muscle bioscaffolds as a tool to study the role of Laminin-211 in the MuSC niche

Pedro Miguel Gameiro dos Santos

Mestrado em Biologia Evolutiva e do Desenvolvimento

Dissertação orientada por:
Professora Doutora Gabriela Rodrigues

2021

"Nature is our biggest ally and greatest inspiration."
Sir David Attenborough, A Life in Our Planet

Acknowledgments

Gostaria de agradecer primeiramente à Professora Gabriela Rodrigues e à Professora Sólveig Thorsteinsdóttir pela oportunidade de poder fazer parte do grupo DEM e desenvolver este trabalho. Foi, com certeza, uma experiência muito enriquecedora.

Obrigado a todos os membros do grupo pela ajuda e acompanhamento contínuo. Ao Luís por todo o apoio na microscopia e à Rita por toda a imprescindível ajuda (e que ajuda!) nos western blots, essa técnica que parece quase magia. Um obrigado especial à Professora Gabriela pela orientação, apoio e compreensão demonstrados ao longo da produção deste trabalho, sem os quais teriam tornado esta tarefa ainda mais complicada.

Ao Telmo pela celeridade na obtenção das imagens de microscopia eletrónica e ao Professor Vítor Sousa pela ajuda na análise estatística.

Aos amigos criados ao longo do meu percurso académico que de uma forma ou outra contribuíram para o meu crescimento pessoal e também para um momento ou outro de diversão pós estudo, claro 😊. Em especial, aos camaradas do mestrado de BED que passaram pelas mesmas "provações". No bed for BED!

Também os meus companheiros de longa data (já lá vão 10 anos), Andreia Monteiro (obrigado pela revisão), Andreia Nunes, Humberto Nicolau, João Silva, Maria Antunes e Ricardo Alves, sem dúvida que facilitaram este trabalho com todo o apoio e boa-disposição.

Finalmente, um grande obrigado à minha família. Aos meus pais, José Augusto Ferreira dos Santos e Célia Maria Pedrosa Gameiro dos Santos, e irmão, André Miguel Gameiro dos Santos, agradeço todo o apoio incondicional e investimento. Espero ter estado à altura!

Por último tenho de agradecer à pessoa que tornou mais fácil e possível a conclusão deste trabalho, muito obrigado Milene Ramos! Espero que sempre assim o seja.

Ao terminar de um ciclo.

Abstract

The extracellular matrix (ECM) plays a crucial role in myogenesis and when disrupted can originate various conditions. When laminin-211 is not present skeletal muscle development is severely impaired leading to Merosin-deficient congenital dystrophy type 1A (MDC1A). Previous works in our group shed some light on the possible origin of this condition occurring during *in utero* development, when secondary myogenesis is undergoing. The absence of laminin-211 seems to lead to an early depletion of the muscle stem cell pool impairing myogenesis. In this work we used embryonic day (E) 18.5 fetus of the dy^W/dy^W mice model and characterized the main ECM proteins in both wild-type and mutant mice. The comparison of both genotypes showed that the absence of laminin α2 may somehow perturb other proteins expression. After characterization, we aimed to produce a system that allowed to study the relative contribution of both sources of laminin-211 (ECM and cells) during skeletal muscle development. We decellularized fetal skeletal muscle, producing a decellularized matrix (dECM) with a similar composition to the native tissue (most importantly laminin-211) but depleted of cellular content. A low concentration SDS treatment, among other component, was optimized to better fulfill this compromise. The dECMs of both genotypes were seeded with C2C12 myoblasts and the cell number and protein production were analyzed. Our results show a tendency to have fewer cells in the mutant dECMs, suggesting that the absence of laminin-211 may difficult C2C12 cells adhesion/proliferation. These cells were able to colonize and contract the dECMs and express different ECM proteins, including laminin-211, opening the possibility for cells to be able to recover a defective niche. This work results in the production of an *in vitro* model representing a possible novel approach to better understand the molecular dynamics of MDC1A and, in the future, the potential development of new therapies.

Keywords: Merosin-deficient congenital dystrophy type 1A, Muscle stem cells, Extracellular matrix, Decellularization, Skeletal muscle

Resumo alargado

A matriz extracelular é o componente não celular de todos os tecidos. Esta estrutura detém não só funções de suporte das células, mas também é um importante mediador de todos os processos biológicos necessários para o correto desenvolvimento dos organismos assim como na manutenção da homeostase. Cada tecido ou órgão apresenta uma matriz extracelular com uma composição distinta. Várias moléculas constituem esta matriz, e é a natureza modelar destas que permite a formação de estruturas com diferentes propriedades mecânicas e bioquímicas, permitindo uma grande diversidade funcional. O desenvolvimento de uma matriz extracelular específica para cada tecido resulta da interação entre células e microambiente, sendo um processo altamente dinâmico e em constante remodelação. A matriz extracelular pode ser dividida em duas principais categorias: a matriz intersticial e as membranas basais. A matriz intersticial é principalmente associada ao tecido conjuntivo e é constituída por proteínas como os colagénios intersticiais, a elastina, fibronectina e proteoglicanos. Estas moléculas atuam com substrato para as células, mas estão envolvidas também na regulação da adesão, migração, proliferação e diferenciação celular. As membranas basais localizam-se mais proximamente das células e devido a isso têm grande influência em como estas interpretam o seu meio. As membranas basais são constituídas essencialmente por colagénio tipo IV, lamininas, nidogénio e perlecan. À semelhança da matriz intersticial, regulam também processos celulares como a proliferação, diferenciação, migração, polarização e sobrevivência ou apoptose. As células recebem informação acerca do seu meio exterior através de recetores membranares.

A matriz extracelular é um fator chave para o correto desenvolvimento de todos os tecidos. A miogénese do músculo esquelético é um exemplo de um processo altamente dependente de sinalização da matriz extracelular. O desenvolvimento do músculo inicia-se cedo durante a embriogénese dos vertebrados com a formação do sómitos. Estas estruturas crescem e desenvolvem-se originando o dermomiótomo. O dermomiótomo possui os percursores miogénicos que irão dar origem ao músculo esquelético. No estádio 8.5 o dermomiótomo "desepiteliza" e células musculares estaminais migram para o espaço abaixo dando origem ao miótomo, iniciando-se assim a miogénese do músculo esquelético. No miótomo desenvolvem-se os mioblastos que proliferam e fundem dando origem aos miotubos. Nesta etapa tanto a presença de fibronectina como de lamininas é crucial para o correto desenvolvimento destas estruturas. No miótomo, as células presentes sofrem diferentes processos reorganizacionais transformando-se em miofibras primárias. A miogénese primária ou embrionária ocorre entre o estádio 11.5 até ao 14.5, a partir do qual se inicia a miogénese secundária ou fetal que decorrer até ao nascimento. Esta fase de miogénese é caracterizada pelo aparecimento das miofibras. Durante a miogénese primária formam-se as miofibras primárias que estabelecem o padrão corporal do músculo esquelético. A miogénese secundária é caracterizada pelo aumento da massa muscular. Este crescimento pode ser dividido em duas fases: células musculares estaminais (Pax7-positivas) podem produzir novos mioblastos que fundem entre si (crescimento por hiperplasia) contribuindo para a formação de miofibras secundárias enquanto outras se diferenciam e fundem com as miofibras primárias levando ao seu crescimento (hipertrofia mediada por células). A ação conjunta destas duas fases leva a um crescimento tanto em número como em tamanho das fibras musculares. Para que este processo ocorra corretamente a presença de laminina-211 parece ser fulcral. A contribuição da matriz extracelular é muito importante para o desenvolvimento dos tecidos e devido a isso, quando esta se encontra perturbada, pode dar origem a diversas patologias. Quando a laminina-211 não está presente o desenvolvimento esquelético muscular é severamente afetado, dando origem à distrofia muscular congénita merosina-negativa (MDC1A), uma das distrofias musculares mais comuns na Europa. Esta condição é provocada por mutações no gene *LAMA2*, responsável pela codificação da cadeia α2 da laminina-221 e -221 levando à produção de uma proteína

não funcional. Os portadores desta doença manifestam diversos sintomas como atrofia e hipotonia muscular, mas também o sistema nervoso parece ser afetado, entre outros sistemas de órgãos. Não existem ainda tratamentos eficazes para esta doença e a maioria do conhecimento existente é proveniente de informação pós-natal, não se conhecendo ainda o momento em que se origina esta condição nem os processos moleculares por detrás da mesma. Estudos anteriores no nosso laboratório revelaram que a origem desta doença poderá ser *in utero* durante a miogénese secundária, onde a ausência de laminina-211 parece levar a uma depleção precoce das células musculares estaminais, não permitindo que ocorra o crescimento das massas musculares.

Este trabalho tem como objetivo acrescentar conhecimento acerca das dinâmicas celulares durante o desenvolvimento fetal desta doença e para isso foi utilizado o modelo de ratinho dy^{W}/ dy^{W} durante o estádio fetal 18.5. Inicialmente começou-se por caracterizar a composição da matriz extracelular de ratinhos normais e distróficos, recorrendo a imuno-histoquímica e western blot. Esta comparação parece demonstrar que a ausência de laminina-211 nos ratinhos distróficos poderá afetar também outras proteínas presentes na matriz extracelular. O colagénio I sofre um aumento de cerca de 3 vezes nos ratinhos mutantes. O aumento desta proteína está documentado em ratinhos após o nascimento e em associação a fibronectina, é responsável por processos inflamatórios e formação de tecido fibrótico (um dos principais sintomas da MDC1A), o que poderá indicar que este sintoma, apesar de não ser observado morfologicamente no feto, poderá iniciar-se ainda *in utero*. No entanto, contrariamente ao expectável, os nossos resultados parecem indicar que existe uma menor quantidade de fibronectina nos ratinhos mutantes. As lamininas parecem também sofrer uma diminuição em quantidade. Após a caracterização da matriz extracelular de ambos os genótipos, propusemo-nos criar um sistema que permitisse estudar a contribuição relativa das duas fontes de laminina-211 (células e matriz extracelular) para o normal desenvolvimento do músculo esquelético. Esta proteína já está presente no nicho das miofibras quando a nova onda de células musculares estaminais entra no programa miogénico. No entanto, estas células parecem também ser capazes de produzir laminina-211 e assim contribuir para a construção do seu nicho. O conhecimento da contribuição relativa de cada uma destas fontes para o normal desenvolvimento do músculo esquelético poderá permitir identificar e desta forma desenvolver terapias para determinados momentos fulcrais para este processo. A descelularização é uma técnica que permite a produção de matrizes extracelulares com uma composição semelhante à do tecido nativo sem a presença de células. Estas matrizes mantêm assim não só a composição química, mas também as suas propriedades mecânicas, o que permite uma maior aproximação ao *in vivo*, apresentando assim várias aplicações terapêuticas. Utilizando esta técnica testámos diferentes protocolos com objetivo de produzir uma matriz descelularizada que mantivesse uma composição semelhante à do músculo inteiro, mas sem células presentes. A utilização do detergente SDS a baixa concentração, em conjunto com outros compostos, permitiu manter na matriz extracelular a maioria das proteínas testadas (especialmente laminina-211) e apenas uma reduzida quantidade de conteúdo celular. No entanto, as matrizes descelularizadas parecem apresentar uma ligeira diminuição na quantidade de proteínas presentes após o protocolo de descelularização. Posteriormente estas matrizes descelularizadas foram cultivadas com células C2C12. Estas células são mioblastos pertencentes a uma linha celular imortalizada originada a partir de células satélite pós-lesão de ratinho, apresentando assim características de células musculares estaminais. A contagem do número de células, após 8 dias em ambos os genótipos, permitiu chegar à conclusão que estas matrizes eram capazes albergar e manter estas células. Os nossos resultados parecem mostrar uma tendência para a presença de um menor número de células nas matrizes descelularizadas mutantes, demonstrando que a ausência de laminina-211 poderá de alguma forma dificultar a adesão ou proliferação das células C2C12. Estas células são capazes de infiltrar nas matrizes e até de contrai-las, mudando-lhes a forma. As células parecem também adquirir propriedades características de células musculares diferenciadas

(alinhamento e afunilamento dos núcleos) assim como também produzem e secretam diferentes proteínas da matriz extracelular como fibronectina, lamininas e especialmente laminina-211. Estes resultados podem indicar que células poderão ter a capacidade de recuperar um nicho incompleto como é o caso da MDC1A. Este trabalho permitiu estabelecer um sistema *in vitro*, que quando otimizado, poderá representar uma nova abordagem para a aquisição de conhecimento acerca das dinâmicas moleculares desta doença durante os estádios fetais, e no futuro, ajudar no desenvolvimento de novas terapias.

Palavras chave: Distrofia muscular congénita merosina-negativa, Células musculares estaminais, Matriz extracelular, Descelularização, Músculo esquelético

Table of contents

List of Figures and Tables

List of abbreviations and acronyms

BM – Basement Membrane
BSA – Bovine Serum Albumin
CMD – Congenital Muscular Dystrophy
dECM – Decellularized extracellular matrix
DMEM – Dulbecco's Modified Eagle's Medium
DNA – Deoxyribonucleic Acid
DNAse – Deoxyribonuclease
DTT – Dithiothreitol
E0.5 – Embryonic day 0.5
E11.5 – Embryonic day 11.5
E12.5 – Embryonic day 12.5
E14.5 – Embryonic day 14.5
E16.5 – Embryonic day 16.5
E17.5 – Embryonic day 17.5
E18.5 – Embryonic day 18.5
E8.5 – Embryonic day 8.5
ECM – Extracellular Matrix
FBS – Fetal Bovine Serum
HRP – Horse Radish Peroxidase
IM – Interstitial Matrix
JAK-STAT – Janus Kinase/Signal Transducers and Activators of Transcription
LAMA2-CMD – Laminin α2 Congenital Muscular Dystrophy
LB – Loading Buffer
MDC1A – Merosin-deficient Congenital Muscular Dystrophy Type 1A
MHC - Myosin Heavy Chain
MIP –Maximum Intensity Projection
MuSC – Muscle Stem Cell
NT – Native tissue
PBS – Phosphate-Buffered Saline
PFA – Paraformaldehyde
PN2 – Postnatal day 2
PVDF – Polyvinylidene Fluoride
SDS-PAGE – Sodium Dodecyl Sulphate-Polyacrylamide Gel Electrophoresis
SEM – Scanning Electron Microscopy
TBST – Tris Buffered Saline 0,1% Tween
TGF-β – Transforming Growth Factor-β
WB – Western Blot
WT – Wild-Type

CHAPTER 1
INTRODUCTION

Introduction

The extracellular matrix (ECM) exists in all tissues and organs. This non-cellular component has crucial importance not only in providing physical scaffolding for cells but is also a key mediator in the chemical and biomechanical processes required for correct tissue morphogenesis, differentiation, and homeostasis maintenance[1].

The appearance of the ECM during evolution is highly correlated with the emergence of multi-cellularity. For organisms to increase in size, the ECM evolved, most likely, to act as structural support and may also have allowed for increased communication between cells. This is illustrated by the high conservation of the proteins present in the ECM[2].

ECM is composed of diverse molecules and each tissue ECM has a unique combination of these conferring them different topologies and properties. The construction of the tissue-specific ECM is a complex process that occurs during tissue development and is the result of dynamic and reciprocal cross-talk between cells and the surrounding microenvironment[3]. One of the most important characteristics of the ECM is its functional diversity. The modular nature of the molecules that constitute ECM and their different properties confer them the ability to create rigid, elastic, wet, or sticky structures that allow highly specialized functions[1].

The importance of the ECM is illustrated by the diversity of cellular and molecular events in which it is crucial (**Figure 1.1**). The ECM confers structural support necessary for correct organ development[4].

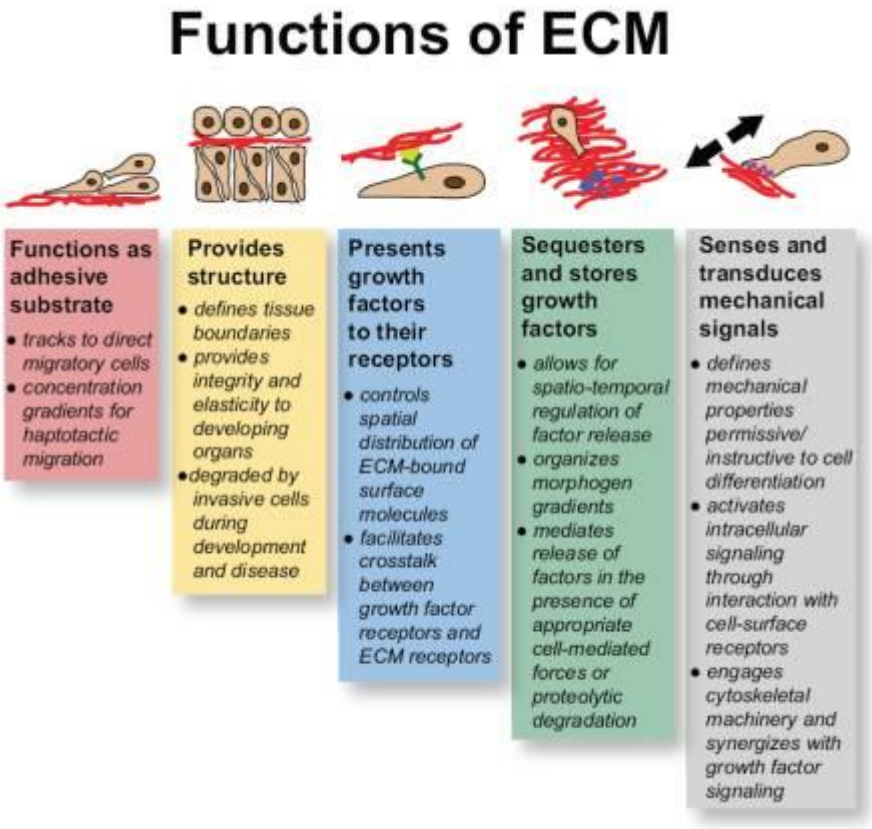

Figure 1. 1 – Main functions of ECM. ECM provides physical support to cells but also acts as a key regulator of the chemical and biomechanical processes involved in major developmental events. From Rozario & DeSimone., 2010.

This highly dynamic matrix can be synthesized or degraded during developmental events or disease[4]. ECM can act as an adhesive subtract used by cells to migrate but can also bind cues forming gradients which promote haptotactic movement in tissue healing[5] and cancer progression[6].

This matrix can modulate cell behavior by facilitating or hampering (acting as a sequester of molecules) the access to paracrine factors, creating morphogen gradients that allow highly accurate spatio-temporal regulation. In response to cell stimuli or aggression, the release of stored factors can also be mediated by the ECM. The ECM is involved in the transduction of mechanical signals that have effects on how cells perceive their surroundings. The ECM is intimately bound to cells through cell-surface receptors that when activated can trigger intracellular signaling pathways giving cells information about their exterior environment and influencing proliferation, differentiation, or cell fate decision[4].

ECM is a tissue- and age-specific structure that is continuously being remodeled and its properties can change over time. ECM remodeling can be achieved by various processes, including synthesis of new components or posttranscriptional changes in already existing ones[7]. Proteolytic degradation can also occur and enzymes such as matrix metalloproteinases and tissue inhibitors of metalloproteinases counterbalance each other to achieve tissue homeostasis. These complex processes are the result of extensive communication between cells and matrix that are mediated by a myriad of growth factors[3].

Extracellular matrix composition

Regarding its biochemical and morphological properties, the ECM can be divided into two major categories: the interstitial matrix (IM) present in connective tissue and the pericellular matrix, most often the basement membranes (BM)[8] (**Figure 1.2**).

The IM is composed essentially by interstitial collagens (mainly types I and III, but also V, VI, VII, XII) and elastin that are important for the structural support of the cells, providing tensile strength and also regulating cell adhesion and migration, consequently mediating tissue development[9]. Fibronectin is another fibril-forming protein that is often associated with the IM, however its action is far more versatile. This protein is present during early development forming a pericellular matrix before BMs are established but is also involved in tissue remodeling, promoting cell attachment and migration[4,8]. Examples of other proteins that constitute this matrix are tenascins that, similarly to fibronectin, are implicated in cell adhesion, migration, and cell growth[10,11]. Proteoglycans, from the chondroitin, heparan, keratan, and dermatan sulfate types, and glycosaminoglycans are also present[12]. These molecules are extremely hydrophilic, which is essential to confer the tissues where these matrices are present their ability to withstand high compressive forces[3,9].

BMs are sheet-like structures that are in close contact with cells, lining epithelial, including endothelial cells, and surrounding muscle, nerve, and fat cells. The main components of BMs are type IV collagen, laminins, nidogen (entactin), and perlecan (a heparan sulfate proteoglycan)[8]. Fibronectin, is also present in close contact with cells in embryonic tissues, often preceding BMs[13]. This protein is very important for the correct polarization of cells and tissue compartmentalization[8].

BMs start to form early in embryonic development, even before implantation[14]. Laminins and collagen type IV self-assemble in a calcium-dependent way and form the core networks of the BMs[15]. Nidogen and perlecan act as binding factors that play a crucial role in bridging these networks, creating a stable structure[16].

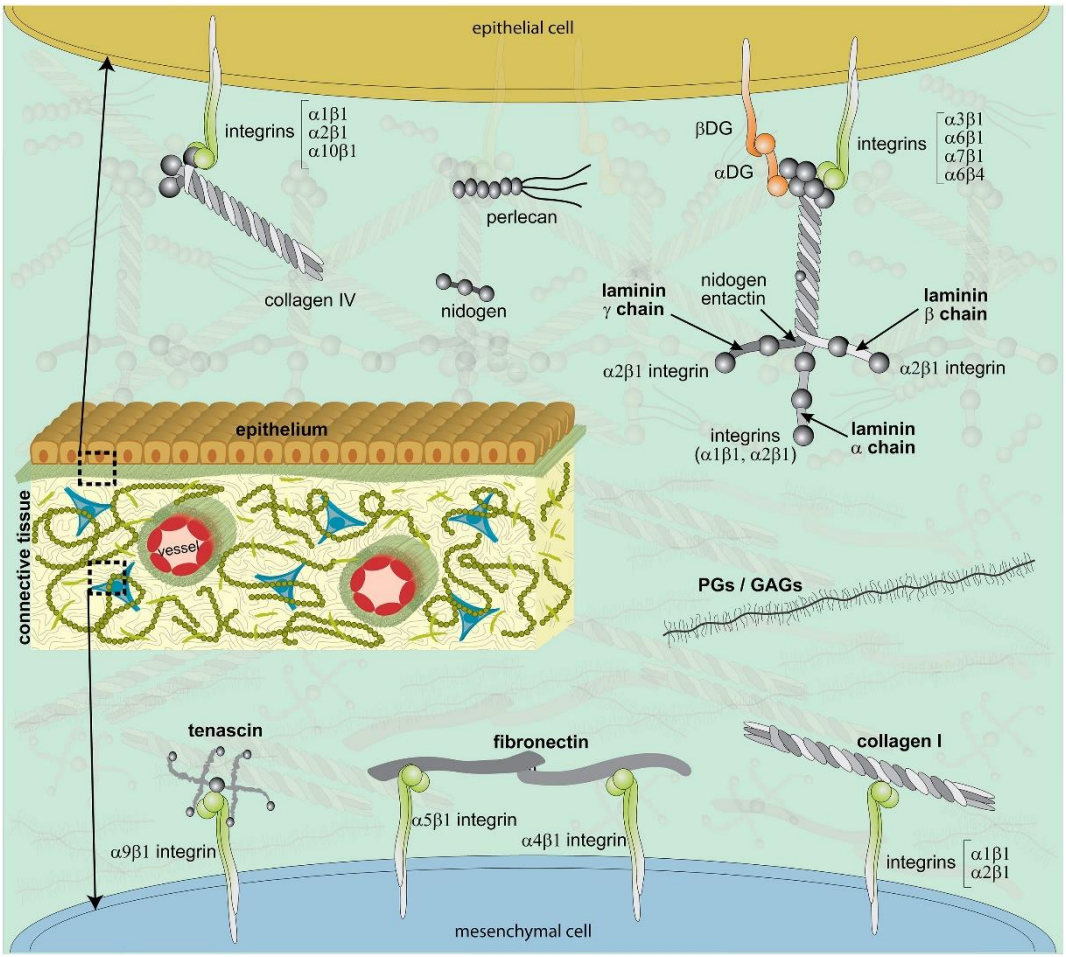

Figure 1. 2 – Basement membrane and interstitial matrix composition. ECM can be divided into two distinct entities regarding their composition and proximity to cells. The major components of BMs (epithelial cell) are in the upper half of the panel and consist of laminins, collagen IV, perlecan, and nidogen. Laminins and collagen IV form a network that incorporates perlecan and nidogen. These molecules then bind to cell membrane receptors such as integrins and dystroglycan (DG). The IM (mesenchymal cell) is composed of various collagens, typified as collagen I, fibronectin, tenascins and, diverse proteoglycans and glycosaminoglycans. Collagens, fibronectin and tenascins interact with cells through integrins. From Thorsteinsdóttir et al., 2011.

Similar to the IM, the BMs act as structural support for cells, although due to their proximity to cells, they have a major influence on how cells interpret their surroundings, actively changing the way cells behave. Key cellular responses such as proliferation, differentiation, migration, polarization, survival, and apoptosis are heavily regulated by the BMs[3,8]. ECM receptors are important players in the regulation of how cells behave in response to certain molecular or mechanical cues. The crosstalk between ECM and cells is mediated by cell surface receptors such as dystroglycan, syndecans and integrins (**Figure 1.2**). These are indispensable for the organization of individual cells into three-dimensional structures[17].

Skeletal Muscle Development and Extracellular matrix contribution

ECM molecules and their receptors on the cell surface mediate major events during development. Skeletal muscle myogenesis is a complex developmental process that is highly dependent on ECM activity[8]. Muscle development starts early in vertebrate embryogenesis with somite formation. These grow and mature giving rise to the dermomyotome. Skeletal muscle myogenesis initiates when cells from the dermomyotome delaminate and differentiate into the first myocytes in the myotome[18]. Dermomyotome cells, in response to different signaling cues, start to express Pax3 and/or Pax7, marking their myogenic potential at embryonic day (E) 8.5[19]. The dermomyotome de-epithelizes and a wave of Pax3- and/or Pax7-positive muscle stem cells (MuSCs) invades the myotome. Ongoing waves of migrating myoblasts from the dermomyotome contribute to the growth of the myotome (**Figure 1.3**). A dorsal BM constituted by laminin-111 and -511, collagen IV and perlecan lines the basal side of the dermomyotome and prevents a precocious myogenic differentiation[20]. Myoblasts can either differentiate and form new myocytes or fuse with pre-existing ones, forming multinucleated myotubes[21]. Fibronectin promotes myoblast adhesion, fusion and proliferation[10,22]. The myogenic program is controlled by myogenic regulatory factors (MRFs) such as Myf5, MyoD, Mrf4, and Myogenin. Myf5, Mrf4 and MyoD are expressed and act as determination factors that set the myogenic fate. Myogenin is expressed later in myogenesis and acts as differentiation factors[23] (**Figure 1.3**).

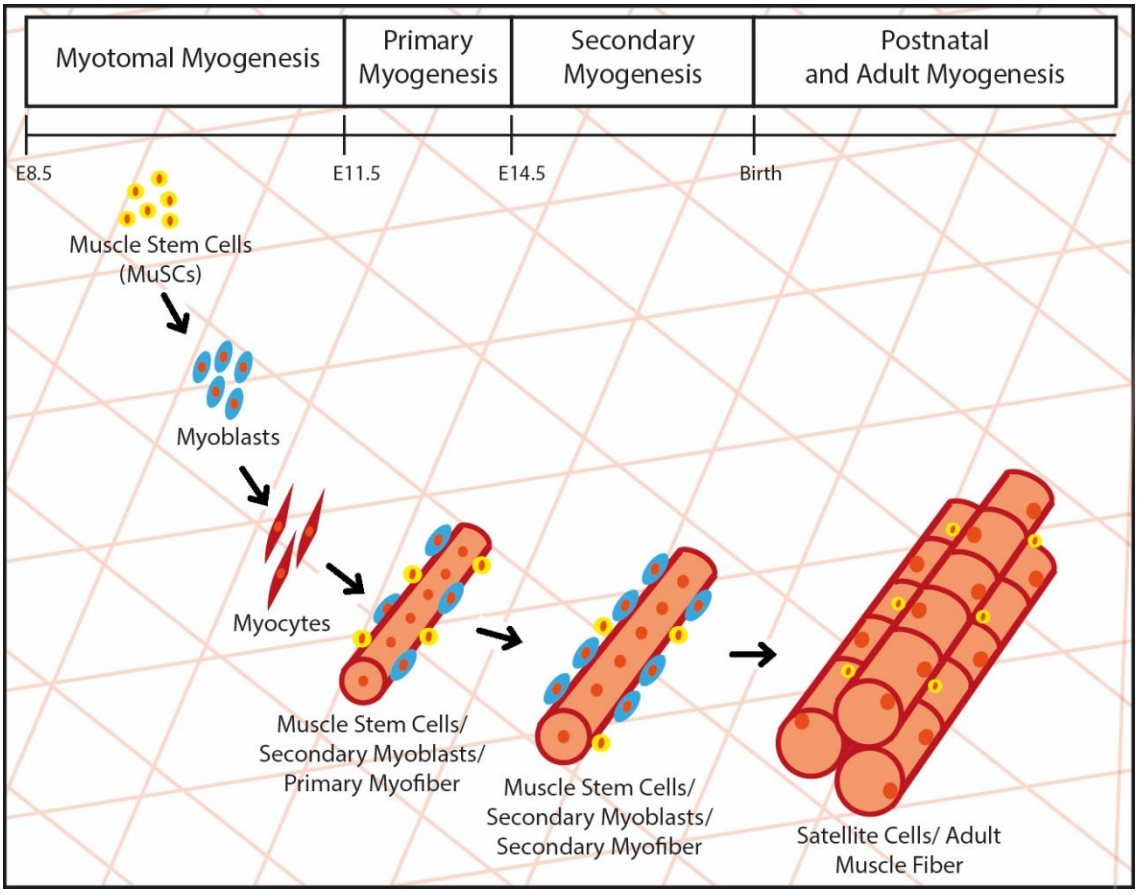

Figure 1. 3 – Skeletal muscle myogenesis throughout time and main cell types present. Pax3- and/or Pax7-positive muscle stem cells delaminate from the dermomyotome and start expressing MRFs such as Myf5, MyoD, Mrf4, and Myogenin and become committed myoblasts. These will differentiate into myocytes in the myotome and fuse with secondary myoblasts originating the primary myofibers. During secondary myogenesis, these myofibers fuse with myocytes, and secondary myoblasts fuse with each other to form the secondary myofibers. After birth, mature myofibers expressing characteristic muscle proteins such as myosin are formed. In the periphery of these muscle fibers, a pool of Pax7-positive satellite cells remains quiescent.

MuSCs can differentiate into myocytes if Myf-5 or MyoD is activated or keep proliferating and constitute a stem cell pool for future muscle growth and development[23]. Myotube formation is strongly impaired in the absence of laminins[24].

The epaxial portion of the myotome will develop into all the epaxial muscle masses (deep back muscles) between E11.5 and E12.5 in mice after undergoing diverse reorganizational processes. The hypaxial portion will give rise to the abdominal and intercostal muscles[25].Myocytes present in the myotome are translocated, re-oriented and elongated and begin to develop into primary myofibers. ECM proteins such as fibronectin and tenascin are present during these steps, suggesting they may play a role in this remodeling[26].

Primary and Secondary Myogenesis

Post-myotomal myogenesis is characterized by the formation of myofibers. This process occurs in two different moments: during primary (embryonic) myogenesis that occurs from E11.5 to E14.5, and the secondary (fetal) myogenesis from E14.5 until birth[27,28] (**Figure 1.4**). As previously stated, ECM is a dynamic structure that is undergoing continuous remodeling. An example is the differential laminin isoform content of skeletal muscle ECM throughout development. During primary myogenesis, there are no assembled laminins present, as time proceeds and the transition to the secondary myogenesis occurs, laminin-211, -411 and -511 begin to be assembled around the myotubes[19]. In the adult, the main isoform present in muscle fibers is laminin-211, with other laminins such as -221, -421 and -521 being circumscribed to the neuromuscular junction area. Laminins are known to be implicated in several processes involved in myogenesis, as it promotes myoblast proliferation, migration, and alignment preceding their fusion[15].

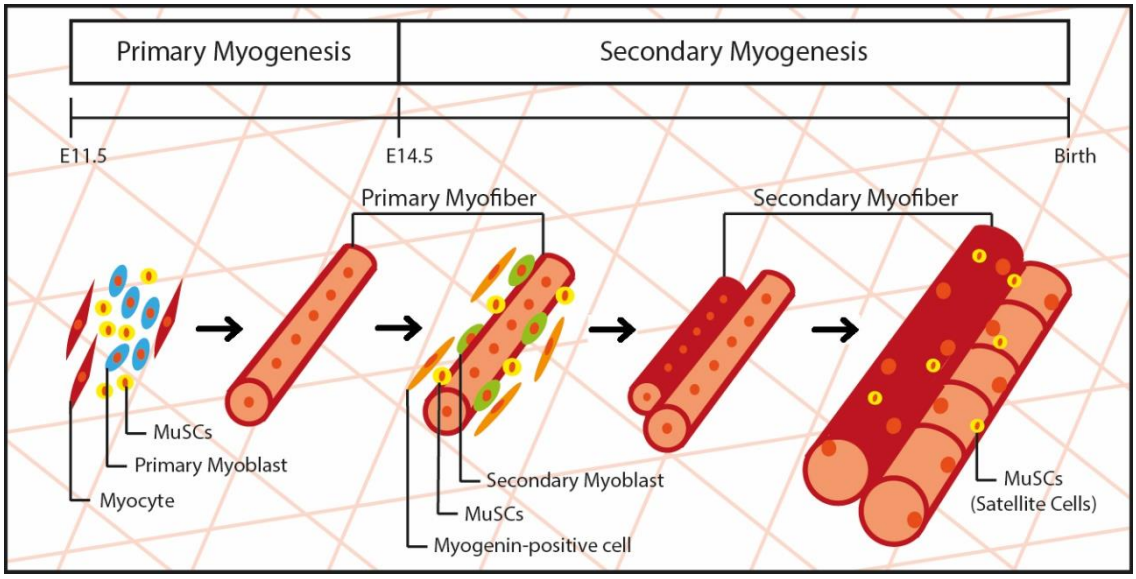

Figure 1. 4 – Primary and Secondary Myogenesis. The formation of myofibers marks the end of post-myotomal myogenesis. Myofibers develop in two distinct moments: during primary (embryonic) myogenesis that occurs from E11.5 to E14.5 and the secondary (fetal) myogenesis from E14.5 till birth. During primary myogenesis, primary myofibers lay the foundation for the body muscle pattern and serve as a basis for future muscle growth that occurs during secondary myogenesis. During secondary myogenesis, MuSCs differentiate into secondary myoblasts that fuse with each other and originate secondary myofibers (growth by hyperplasia) but also differentiate into myocytes that will fuse with existing myofibers increasing their size (cell-mediated hypertrophy).

Primary myogenesis initiates when Pax3- and/or Pax7-positive MuSCs differentiate into myoblasts that fuse with the myotomal myocytes or to each other forming the primary myotubes in the

trunk. In the limbs, tongue and diaphragm, myoblasts fuse with each other and originate primary myotubes. The basic muscle pattern of the body is established by this process[18].

During secondary myogenesis, a second wave of MuSCs (expressing Pax7 only) differentiates into secondary myoblasts and fuses with the pre-existing (primary) myofibers near their innervation site[29]. Pax-7 positive MuSCs are initially localized among primary myofibers and contribute to the formation of new secondary myofibers by dividing and producing new myoblasts that fuse with each other (growth by hyperplasia). In this ongoing process, some of these MuSCs will differentiate and give rise to new myocytes that will fuse with the existing myofibers, increasing their size (cell-mediated hypertrophy). These two phases of muscle growth during secondary myogenesis are responsible for both an increase in myofiber number and size, leading to growth in muscle mass[19,28] (**Figure 1.4**).

Between E16.5 and E17.5, Pax7-positive MuSCs start becoming located under the BM surrounding myofibers, and by E18.5 all these cells are thought to have entered their niche[19]. The pool of MuSCs that is enclosed under the BM of muscle fibers will, in the adult muscle, be called satellite cells due to their characteristic location. In the adult, these cells enter quiescence and are only activated in case of injury[30].

Extracellular matrix and disease

The importance of the ECM for the correct development and function of tissues is illustrated by the myriad of diseases associated with a defective ECM. Mutations in ECM proteins codifying genes result in an extensive range of serious inherited disorders. These include skeletal dysplasias, chondrodysplasias, epidermolysis bullosa, Ehlers–Danlos syndrome, Alport syndrome and various forms of muscular dystrophy[31].

Muscle dystrophies can be the result of pathological changes in the muscle ECM. Genetic studies of several muscle diseases show that the BM is critical for the maintenance of muscle integrity. In all these diseases, skeletal muscle tissue is affected and characterized by progressive muscle weakness, fibrosis, and fat infiltration. Muscle dystrophies can result from the loss or impairment of any of the elements in the ECM-cytoskeleton linkage[32].

The examples include laminin α2 (merosin-deficient congenital muscular dystrophy type 1A (MDC1A)) and its transmembrane receptors, integrin α7 (congenital myopathy) and dystroglycan (various dystroglycanopathies), dystrophin (Duchenne and Becker muscular dystrophy), collagen IV (Walker Warburg syndrome, also associated with dystroglycan mutations), and the α chains of collagen VI (Ullrich congenital muscular dystrophy and Bethlem myopathy). For muscle maintenance, both structural and signaling properties of the BM are required[33,34].

Merosin-deficient congenital muscular dystrophy type 1A

MCD1A is a form of congenital muscular dystrophy, also known as laminin-α2 CMD (LAMA2-CMD), caused by a mutation in the *LAMA2* gene. This gene is responsible for encoding the laminin α2 chain, present in laminin-211 and laminin-221. The disease has an autosomal recessive inheritance, with individuals with two dysfunctional copies displaying the disease[35].

As previously stated, laminin-211 is the main isoform present in the BM that surrounds muscle fibers, while laminin-221 is mostly found at the neuromuscular junction. The absence of a functional laminin-211 and -221 results in a disruption of the crosstalk between the ECM and the muscle fiber cytoskeleton, causing structural instability and, as a consequence, muscle fiber degeneration or in a defect during myogenesis that results in impaired muscle growth. The development of the disease can be the result of one of the aforementioned factors or the combination of both[19,36]. Laminin-411 and -511

act as compensators but are inadequate substitutes and are unable to recover normal ECM integrity and signaling[37].

Patients show a milder to severe phenotype depending on the degree of the laminin α2 chain deficiency. This disease is characterized by an array of symptoms which include severe muscle hypotonia, atrophy of the muscles of the limbs, back and face, associated with contractures that affect the joints, mainly the elbows, hips, knees, and ankles. The diaphragm can also be affected which can lead to respiratory failure. The patients display severe muscle weakness along with problems in the spine, such as scoliosis. Due to these clinical features locomotion is severely affected. The absence of laminin-211 and -221 affects a range of tissues besides skeletal muscle, including the central nervous system, the peripheral nervous system and heart[36,38].

MCD1A, although being a rare disease, accounts for approximately 30% of the cases of congenital muscular dystrophy in Europe. To date there is no treatment available with patients having a life expectancy as low as a decade, thus representing the urgency in better understanding the underlying mechanisms that cause this disease[39].

Several mouse models are used to study laminin α2 deficiency. Cure CMD (www.curecmd.org) recommends the dy^W/dy^W ($dy^{W-/-}$) mouse as a model of MDC1A. These mice are a knock-out line that only expresses a small amount of truncated α2 chain rendering it non-functional[36]. Using this model Nunes et al.[19] showed for the first time that this disease starts to manifest i*n utero* during the development of the fetus, as the result of a defect in (secondary) myogenesis. Although MDC1A is characterized by generalized inflammation and the formation of fibrotic tissue, during the fetal stages there are no signs of these symptoms. The malformation of the muscle seems to be due to a precocious reduction in the number of Pax7-positive MuSCs and differentiating Myogenin-positive myoblasts, resulting in impaired muscle growth in $dy^{W-/-}$ fetuses[19]. In the adult $dy^{W-/-}$, MuSC also show reduced expansion ability after injury, resulting in muscles with low regenerative potential[36].

The expansion step fails during secondary myogenesis in $dy^{W-/-}$ fetuses. There is no more apoptosis in fetal $dy^{W-/-}$ myofibers. Wild-type (WT) and $dy^{W-/-}$ fetuses have the same number of myofibers (although these are smaller in the $dy^{W-/-}$). The onset of this disease appears to occur at or soon after E17.5 when MuSCs begin to fail to expand at the same rate as they do in the WT. This lower expansion rate continues until E18.5, resulting in smaller muscle masses. At postnatal day 2 (PN2), the rate of expansion appears similar to the WT. However, it is not enough to rescue muscle growth[19] (**Figure 1.5**).

These data lead to the hypothesis that laminin-211/221 has a crucial role in regulating fetal MuSCs, promoting their self-renewing potential and preventing precocious differentiation, since both processes are impaired in $dy^{W-/-}$ MuSCs. MuSCs amplification occurs when Pax7-positive cells undergo symmetric cell divisions and originate two new Pax7-positive cells. When the cell division is asymmetric only one Pax7-positive stem cell is formed and simultaneously a committed cell which will later differentiate and fuse with myofibers[19,40] (**Figure 1.5**). One possible interpretation of these data could be that in the absence of these proteins the complex balance of symmetric and asymmetric divisions in MuSCs is shifted, resulting in early depletion of the stem cell pool. Although the mechanism underlying this regulation is still unknown, RT-qPCR analysis of fetal muscles implied JAK-STAT and myostatin as possible candidate pathways involved in this process[19].

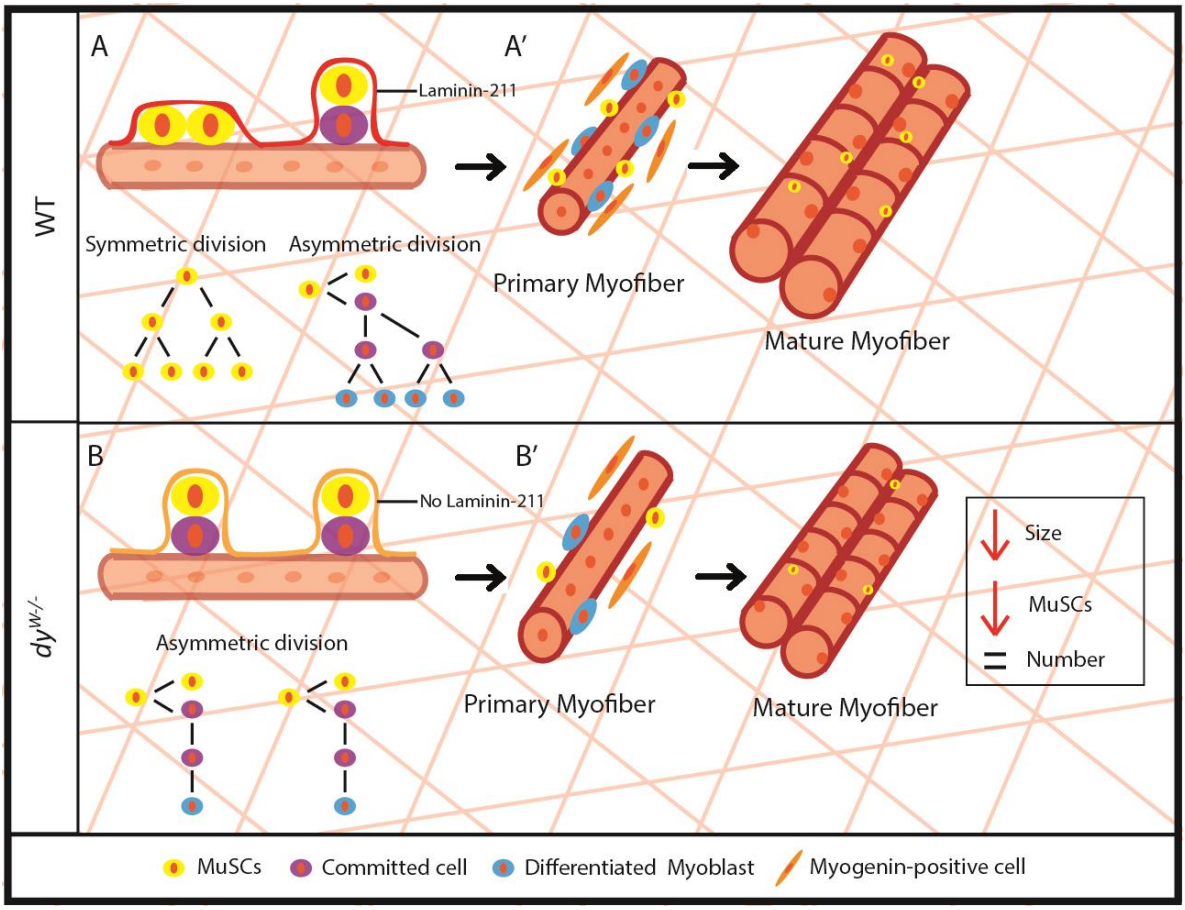

Figure 1. 5 – Early stem cell pool depletion leads to impaired skeletal muscle development in *dy*$^{W-/-}$. Laminin-211 presence is necessary for correct skeletal muscle development (WT, **A-A'**). Laminin-211 signaling regulates MuSCs ratio of symmetric and asymmetric divisions (**A**) ensuring that the stem cell pool is not depleted and muscle growth. Symmetric divisions originate two MuSCs while asymmetric give rise to one MuSC and one committed cell that will differentiate into a myoblast. In the *dy*$^{W-/-}$ (**B-B'**) there is no laminin-211 present which results in the deregulation of the previously mentioned ratio resulting in more asymmetric divisions (**B**) which depletes the stem cell pool but also less committed cells and consequently, less differentiated myoblasts. This results in fewer Myogenin-positive cells which will lead to a reduction of myofibers' size (**B'**) when compared to the WT (**A'**). Myofibers' numbers are the same in both conditions. *dy*$^{W-/-}$ also show a decrease in satellite cell number which hampers the regenerative potential of the muscle.

Decellularization of fetal skeletal muscle

Decellularization is an experimental technique that removes the cellular content of the tissue and produces a tissue-specific ECM scaffold that can accurately mimic the natural tissue microenvironment to a higher degree when compared to engineered natural or synthetic materials[41]. The use of decellularized matrices (dECM) has many scientific and clinical advantages. Decellularized bioscaffolds models *in vitro* show more *in vivo*-like responses than the traditional 2D *in vitro* models. These 2D models seeded in glass/plastic limit cell-cell and cell-ECM interactions altering cell responses. The 3D nature of the decellularized structures and the maintenance of the molecular and mechanical properties make these models better alternatives to understand the molecular dynamics in the NTs[42]. This is illustrated in a series of studies in the most diverse organ systems[43–49]. The ability of dECMs to recapitulate NT microenvironments holds great potential for *in vitro* studies of diverse disease phenotypes but also tissue responses to drugs or toxins[42].

These dECMs also have many therapeutic applications. Due to the removal of cell content and antigenic components, the immune responses upon transplantation are minimized[50].

The maintenance of the original ECM composition and architecture of tissues facilitates cell adhesion, proliferation, and differentiation[42]. Many commercial products harvested from allogeneic or xenogeneic tissue sources are used today in clinics for regenerative purposes[41].

Our group has been working with the aim of unveiling the molecular and cellular dynamics involved in the onset of MDC1A. Previous studies in our lab (unpublished data) showed that in a healthy mouse fetus, when MuSCs enter their niche at E17.5, the pre-existing myofibers have already generated a niche containing laminin-211. We additionally found that MuSCs may also produce laminin-211 (unpublished data) and therefore may contribute to the construction of their niche. More detailed knowledge on the relative importance of these sources of laminin-211 could contribute to the development of new target-oriented therapies.

Silva et al.[44] used a decellularization setup in fetal heart that showed the potential of dECMs for supporting and maintaining necessary cues for fetal cardiomyocytes development. In the present work we replicated this experimental setup in skeletal muscle and isolated a cell content free ECM. The decellularization of fetal skeletal muscle produces an dECM containing laminin-211 (or not in the $dy^{W-/-}$) allowing for recellularization with MuSCs. dECMs preserve necessary ECM cues needed for the normal muscle development. The analysis of how the seeded cells behave (depending on both their genotype and the decellularized ECM's one) could give an insight on the relative contribution of each source (cells or ECM) of laminin-211 for the normal skeletal muscle development.

As previously stated, normal muscle development is dependent on the correct ratio between symmetric and asymmetric divisions of Pax7-positive MuSCs. It is plausible that the regulation of this ratio may be altered in the mutants resulting in early depletion of the stem cell pool[19] (**Figure 1.5**). This model could be an *in vitro* approach to better understand the MuSCs proliferation/differentiation dynamics that seem to be altered in the $dy^{W-/-}$ mice as showed by Nunes et al.[19]. With this setup, we want to understand the relative influence of both the MuSCs and myoblasts and their microenvironment for the correct development of the muscle and what fails in the context of MDC1A using the mutant $dy^{W-/-}$ mice model.

A deeper knowledge of the interactions between muscle cells and their ECM is paramount for the development of therapies that can efficiently target the key processes of the onset of diseases such as MDC1A.

Aims of this thesis

In this work we aim to characterize the skeletal muscle ECM of fetal $dy^{W-/-}$ mice in comparison to the WT condition to gain further understanding of ECM composition in the context of MDC1A. After this characterization, we aim to develop a protocol to produce dECMs that preserve the main components of the ECM (including laminin-211) and finally, recellularize these matrices with myoblasts and assess their number and ECM proteins expression in the presence or absence of laminin-211. As mentioned above, a better understanding of what fails in the context of MDC1A is imperative for the development of new therapies.

CHAPTER 2
MATERIALS AND METHODS

Materials and Methods

Embryo collection

E18.5 homozygous $dy^{W-/-}$ mutants and WT fetuses were obtained by crossing heterozygous C57BL/6N dy^{W} mice. This mouse strain has a *LacZ-neo* cassette inserted in the *LAMA2* gene and the homozygous animals only produce a truncated form of laminin α2 protein missing the N-terminal LN domain rendering it non-functional[36,51].

Pregnancies were assessed through the observation of the copulation plugs and the morning of the plug was designated E0.5. Pregnant females were anesthetized via inhalation of isoflurane (2-chloro-2-(difluoromethoxy)-1,1,1-trifluoro-ethane) and confirmed unconscious by lack of a withdrawal reflex upon toe pinch. These females were then sacrificed by cervical dislocation.

Fetuses were removed from the uterus in ice-chilled phosphate-buffered saline (PBS, composition in **Annex I – P2**), beheaded and processed. The deep back muscles were isolated and used in the different experimental setups or kept at 4ºC in PBS or at -80ºC for short or long-term preservation, respectively. When used in cell culture, the fetal muscles were isolated under sterile conditions in a laminar flow hood. The described procedures were approved by the national competent authority.

Genotyping

DNA was extracted from tail snips of E18.5 fetuses from heterozygous dy^{W} crossings and genotyped using the following primers: 5' ACTGCCCTTTCTCACCCACCCTT 3', 5' GTTGATGCGCTTGGGACTG 3' and 5' GTCGACGACGACAGTACTGGCCTCAG 3'. Protocol adapted from elsewhere[52]. Protocol in **Annex I – P1**.

Tissue decellularization

Freshly removed muscles were washed in PBS to remove any residual blood and promptly submitted to the decellularization protocol. When muscles had been previously stored at -80ºC, the tissue was thawed in PBS in a Petri dish on ice. The decellularization protocol consists of a 3-day protocol described elsewhere[44] which we adapted to the skeletal muscles under study. Protocol in **Annex I – P2**.

On day 1, samples were incubated in 3mL of Hypotonic Buffer in a 12-well plate for 18h. The next day, samples were washed 3 times in PBS for 1h each and then incubated in 3mL of different percentages Sodium Dodecyl Sulfate (SDS) (0.02%, 0,05% and 0,2%) or Triton X-100 (0,2%, 0,5%) in Hypotonic Wash Buffer solutions for 24h. These different treatments were used to select the best one in terms of decellularization efficiency. On the last day, the samples were washed 3 times for 20min with 3mL of Hypotonic Wash Buffer and incubated with 1mL of DNase treatment for 3h at 37ºC. The dECMs were then washed with PBS 3 times for 20min each, followed by an overnight final wash with slow agitation (60rpm). All procedures were performed at 25ºC and with agitation (170rpm) unless otherwise stated. Solutions in **Annex I – P2**.

The resulting dECMs were then used immediately or stored at 4ºC in PBS or cryopreserved at -80ºC for short or long-term storage, respectively. When the final application of the matrices was cell culture, all the previous procedures were performed under sterile conditions in a laminar flow hood and the solutions were sterilized (by steam sterilization or filtration) and Penicillin/Streptomycin added (10µL per 1000µL).

Immunohistochemistry - Cryosections

a. Embedding of samples for Cryosectioning

The isolated deep back muscles (referred as native tissue) or dECMs from WT and mutant E18.5 mice were fixed in 4% paraformaldehyde (PFA) in 0.12M phosphate buffer with 4% sucrose for at least 4h at 4ºC, washed and then submitted to solutions with an increasing gradient of sucrose: solution 1 (0.12M phosphate buffer with 4% sucrose) and solution 2 (0.12M phosphate buffer with 15% sucrose), each overnight or over day at 4ºC. After that, the samples were incubated at 37ºC for 3h in a third solution (0.12M phosphate buffer with 15% sucrose and 7.5% gelatin) and frozen in small aluminum boats on top of dry ice-chilled or liquid nitrogen-chilled isopentane and stored at -80ºC. The protocol was adapted from elsewhere[53]. Protocol in **Annex I – P3**.

b. Cryosectioning and Antibody Incubation

The frozen cubes containing the samples were mounted with O.C.T. compound (Tissue-Tek) in a Leica CM1860 Cryostat and cut into sections of 12µm. The cryosections were collected on Super Frost slides and processed for immunohistochemistry. The sections were left to dry for 1h at room temperature and then washed 3 times with PBS for 10min each.

The blocking step consisted of a 5% Bovine Serum Albumin (BSA) in PBS solution for 30min and then diluting the primary and secondary antibodies in 1% BSA in PBS.

The incubation in the primary antibodies was performed overnight at 4ºC. Sections were then washed 3 times (10 min each) in PBS and incubated in the secondary antibody at room temperature for 1h30. After the secondary antibody, slides were washed 3 times (10 min each) in 4X PBS. The use of a fourfold concentrated PBS has been shown to reduce the unspecific binding of the secondary antibody to the tissue. The nuclear staining was obtained soaking the slides for 30secs in DAPI (4′,6-diamidino-2-phenylindole). The slides were then washed in PBS, mounted in anti-fading medium (50mg/ml n-propyl-gallate in PBS:glycerol (1:9)) and finally sealed with a coverslip. All the antibodies and respective dilutions used, are listed in **Annex II – Table S1**. The secondary antibody negative controls are in **Annex II – Figure S1**. The slides were stored at 4ºC until image acquisition. The protocol was adapted from elsewhere[19]. Protocol in **Annex I – P3**.

The immunohistochemistry results were observed in an Olympus BX60 fluorescence microscope and images acquired using a Hamamatsu Orca R2 camera.

Scanning electron Microscopy

WT and mutant dECMs and NT were fixed in a mixture of 2.5% glutaraldehyde and 4% PFA diluted in phosphate buffer for 6h at 4ºC. The samples were then washed with the dilution buffer and dehydration was achieved by following a protocol of incubation in vials with an increasing gradient of ethanol (30%, 50%, 70%, 80%, 90%, and 100%) for 15 min each under agitation, excluding the last concentration that was renewed 3 times (15min each). Afterward, the samples were transferred to vials containing acetone until dehydration in a critical point dryer.

Later, the samples were coated with gold salts and the images acquired using a JEOL JSM-5200LV electron microscope. Protocol in **Annex I – P4**.

Western Blot analysis

a. Protein Extraction

dECMs and NT from WT and mutant mouse fetuses were thawed on ice and added to individual 2mL Eppendorf tubes containing 2X Sodium Dodecyl Sulphate-Polyacrylamide Gel Electrophoresis (SDS-PAGE) loading buffer (LB) with freshly added 100mM dithiothreitol (DTT). The protein extraction was made directly in LB, avoiding the loss of protein. Samples were then homogenized using one tungsten carbide bead in a Retsch MM 400 mixer mill for 5min. After that, the tubes containing NT were sonicated in an ultrasound bath for another 5min to denature the DNA present in the extractions. All samples were then heated for 10min at 50ºC and centrifuged (13000rpm) for 15min at 4ºC. Finally, the supernatant was transferred to fresh tubes and protein concentration measured using Nanodrop 1000 Protein Abs 280nm function. The samples were kept at -20ºC until further use. Solutions and protocol in **Annex I – P5**.

b. Polyacrylamide gel Electrophoresis

The proteins studied have a range of high molecular weights so low percentage gels were used to run these samples. Proteins in the higher end of this range were run in 6% acrylamide gels and at the lower end in 8% acrylamide gels. In each gel 50µg of the protein and 10 µL of HiMark™ Pre-stained Protein Standard (Invitrogen) were loaded. Runs were made in an electrophoresis tank containing Running Buffer for 80min with constant voltage, 10min at 150V and 70min at 175V. Gels from both percentages were run in parallel in the same electrophoresis tank at the same time, under the same conditions. Solutions and protocol in **Annex I – P5**.

c. Transfer

After electrophoresis, gels and the activated polyvinylidene fluoride (PVDF) membranes were mounted in a transfer cassette and transfer occurred in chilled Transfer Buffer containing 20% methanol and 0.05% SDS in an electrophoresis tank on ice (to prevent the gel from melting). The runs had 90min of duration at 100V.

After the transfer, the gels were stained with BlueSafe (NZYTech) and the quality of the transfer was assessed by the staining profile.

d. Antibody incubation

Membranes were incubated in a blocking solution of Tris Buffered Saline with 0,1% Tween (TBST) with 5% milk for 1h with agitation and rinsed 3 times with TBST before overnight incubation with the primary antibodies (diluted in TBST with 5% BSA and 0.01% sodium azide) with agitation in a cold chamber (4ºC). The following day, the membranes were washed for 5min with TBST and incubated with Horse Radish Peroxidase (HRP)-conjugated secondary antibodies (diluted in TBST with 5% milk) for 1h at room temperature. All the antibodies and respective dilutions used are listed in **Annex II – Table S1**. Later, the membranes were washed 3 times (5min each) with TBST and kept submerged in it until developed. After development, the former antibodies were stripped by washing 3 times for 5min with TBST and the same protocol mentioned above was repeated with a new set of antibodies.

e. Membrane development and quantification

The incubated membranes were developed using Pierce™ ECL Western Blotting Substrate developing kit and the images acquired in a Bio-Rad ChemiDoc XRS+ System.

When all the bands of interest were obtained the membranes were incubated with Ponceau Red (15min) and the lane staining profile was digitalized (lane staining profile in **Annex III – Figure S2**).

Plots of the bands of interest were traced and their area measured using Fiji Wand Tool. The same procedure was performed in the Ponceau Red stained membranes.

Cell culture in decellularized matrices

a. Cell culture

dECMs of all genotypes were cut into pieces of approximately 500x500x200µm and left to soak in DMEM (Dulbecco's Modified Eagle's Medium) with 10% Fetal Bovine Serum (FBS) and Penicillin/Streptomycin added (10µL per 1000µL) for to 2h in a 96-well plate (3 pieces per well).

The culture medium was then removed and 50000 C2C12 cells[54] suspended in fresh medium were added to the matrices in each well. The cell number was counted using a hemocytometer and the cell viability assessed with the trypan blue dye assay.

After 2 days of incubation, the dECMs, now containing the cells, were transferred to a 48-well plate and the medium was refreshed every two days until the desired timepoint, 8 days or 15 days. The cultures were kept at 37ºC with constant humidity in a cell culture incubator with 5% CO_2. Protocol in **Annex I – P6**.

All the procedures were conducted under sterile conditions in a laminar flow hood in the cell culture facility.

b. In toto immunohistochemistry

After the desired timepoint was reached, the pieces of matrices were harvested from the cell culture wells and processed for immunohistochemistry. The samples were fixed in 2% PFA in phosphate buffer for 2h at 4ºC. The antibody staining protocol was the same as the one described in the previous section (see "Immunohistochemistry"). Nuclei were stained with DAPI and Methyl green. The pieces were then mounted in anti-fading medium (50mg/ml propyl gallate in PBS:glycerol (1:9)) in the center of metal rings enclosed in-between two coverslips attached with beeswax. All the antibodies and respective dilutions that were used are listed in **Annex II – Table S1**. The secondary antibody negative controls are in **Annex II – Figure S1**.

Immunohistochemistry image stacks of 100µm of the matrices were obtained in a Leica SPE confocal microscope system.

Image analysis and Quantifications

All images were processed and analyzed in Fiji software (version 2.0.0-rc-67/1.52d).

Confocal image stacks of 100µm were compressed into one maximum intensity projection (MIP) image resorting to the Maximum Intensity Z-projection Plugin (https://imagej.net/Z-functions) in Fiji. Filters were applied to enhance the user visualization (Median, radius=3 and Gaussian Blur, sigma=1) of cell nuclei and the brightness and contrast adjusted for the same reason. Cell quantifications in the matrices were performed using Fiji Plugin Cell Counter (https://imagej.net/Cell_Counter). A 180x180µm area was established for all MIPs and the cells (nuclear staining was used as a proxy) in that area were counted (**Figure 2.1**). The areas used for cell counts were selected based on similar immunostaining intensity. All images were counted in a blind trial procedure, without knowing the genotype, to minimize user effect.

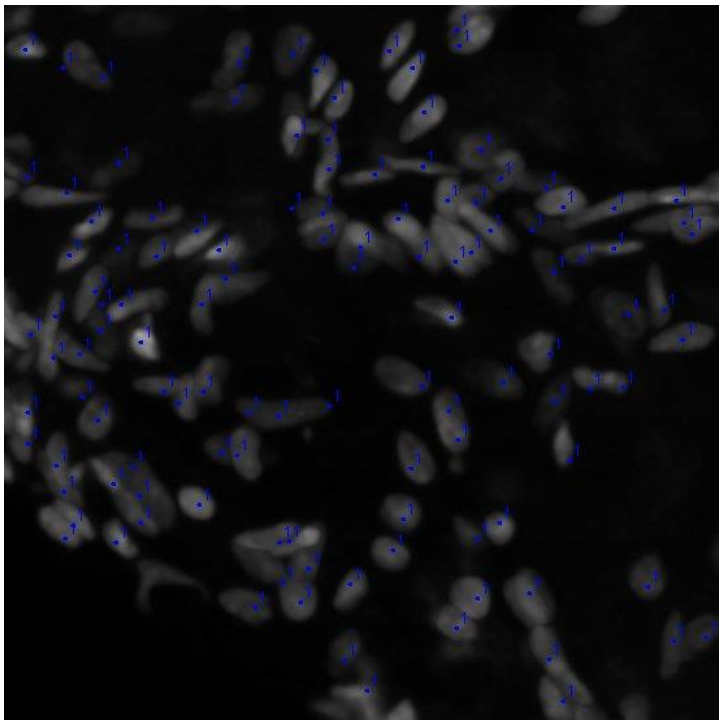

Figure 2. 1 – Cell counter window example. Nuclear staining was used as a proxy for the number of cells. Each blue dot corresponds to a cell.

Statistical analysis

All statistical techniques were applied using R software (version 4.0.0) and Microsoft Excel.

Samples were tested for normality using Shapiro-Wilk test and for homogeneity of variances using Bartlett's test. Then a one-way ANOVA was performed using the ANOVA function in R software.

CHAPTER 3
RESULTS

Results

ECM proteins deposition seems to be disturbed in the absence of Laminin α2

Given the fact that the ECM is a highly interlinked structure, it is possible that the lack of functional laminin-211 could affect the accumulation or organization of other ECM molecules. To address this question, we used immunohistochemistry and western blot (WB) analysis to characterize the ECM of fetal deep back muscles of E18.5 $dy^{W-/-}$ compared to that of WT mouse fetuses. The choice of this stage coincides with the earliest manifestation of a myogenesis defect caused by the absence of laminin-211[19].

First, we studied the distribution of key ECM proteins in E18.5 WT fetuses compared to same stage $dy^{W-/-}$ fetuses by using immunohistochemistry on cryosections of deep back muscles.

In the WT, fibronectin is present in the space between myofibers (magenta asterisks), which can be visualized with myosin heavy chain (MHC) antibody staining (**Figure 3.1**A'' and A''', yellow arrows, magenta asterisks). Fibronectin immunostaining in the $dy^{W-/-}$ seems to be fainter than in the WT (compare **Figure 3.1**A'' and A''' with B'' and B''', yellow arrows) but with a similar location.

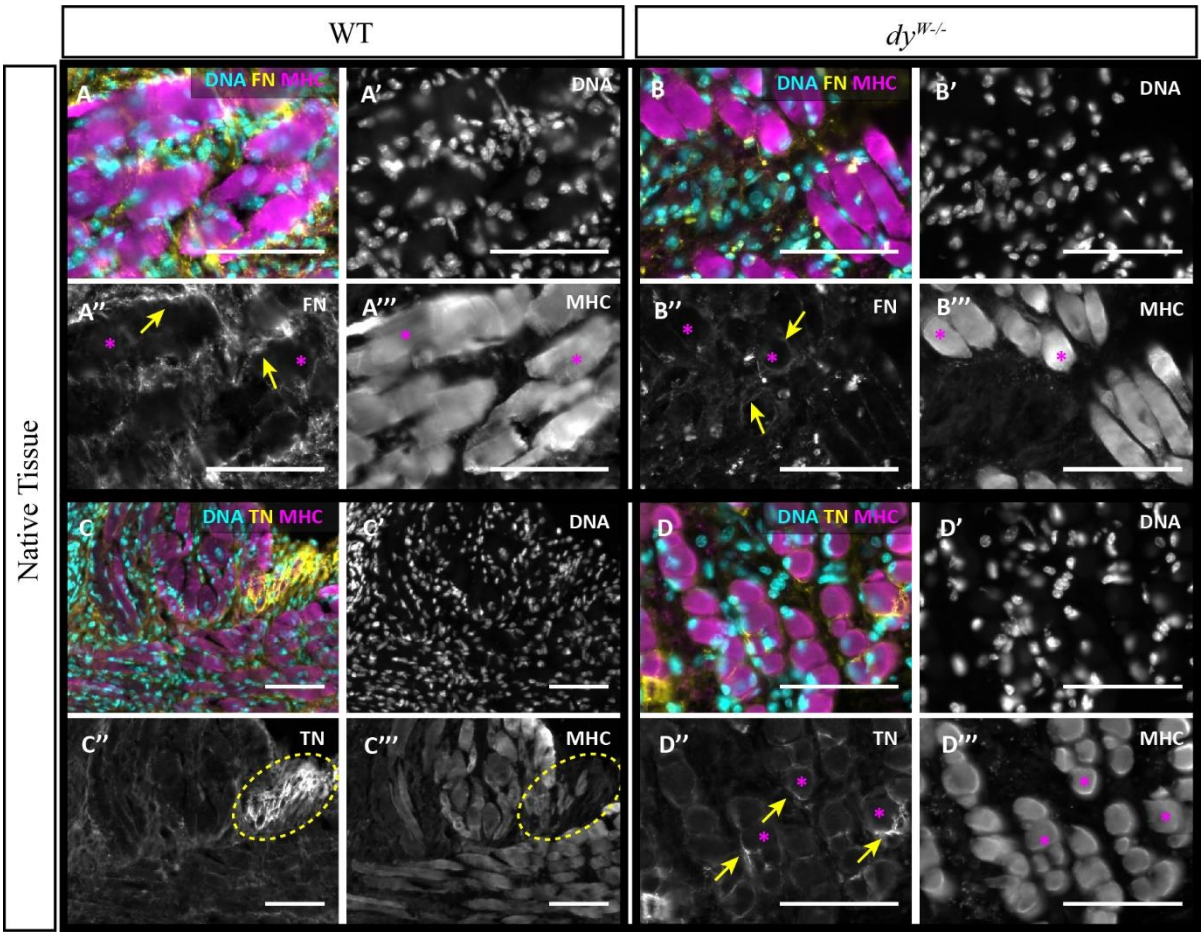

Figure 3. 1 – Characterization of the distribution of fibronectin and tenascin in WT and $dy^{W-/-}$ E18.5 mouse fetuses deep back muscles. Cryosections of NT from WT and $dy^{W-/-}$ E18.5 fetuses processed for immunofluorescence. Immunostaining for fibronectin (FN) (**A** and **B**, yellow; **A''** and **B''**, grayscale), tenascin (TN) (**C** and **D**, yellow; **C''** and **D''**, grayscale), myosin heavy chain (MHC) (**A**, **B**, **C**, **D**, magenta; **A'''**, **B'''**, **C'''**, **D'''**, grayscale) and DNA (**A**, **B**, **C**, **D**, cyan; **A'**, **B'**, **C'**, **D'**, grayscale). Magenta asterisks correspond to the same myofibers (**A''** and **A'''**, **B''** and **B'''**, **D''** and **D'''**). The color image (**A**, **B, C**, **D**) is a merge of the respective grayscale channels. Arrows, asterisks and circles represent staining of interest with the same color. Scale bars: 75µm.

The tenascin staining pattern is similar in both genotypes (**Figure 3.1**C-C''' and D-D'''). Tenascin (**Figure 3.1**C'' and C''', yellow circle and D'', yellow arrows) seems to be localized near the MHC antibody stained myofibers (**Figure 3.1**C''and C''', yellow circle represents the same area), being the tenascin staining location more visible in $dy^{W-/-}$ (**Figure 3.1**D''and D''', yellow arrows near magenta asterisks). In the WT the higher intensity of tenascin staining and lower intensity of MHC staining could correspond to a tendon (**Figure 3.1**C''-C''', yellow circle).

The immunohistochemistry staining experiments in **Figure 3.1** suggest that fibronectin immunostaining is reduced in the $dy^{W-/-}$ when compared to WT (**Figure 3.1**B-B''' and A-A''', respectively), while tenascin seems to have a similar distribution in both genotypes.

We next analyzed the staining pattern of proteins present in the BM surrounding muscle fibers. In skeletal muscle, laminin-211 binds to collagen IV to form the core network of the BM[8]. To determine whether collagen IV deposition is affected by the lack of laminin-211 in the $dy^{W-/-}$, we immunostained sections from both genotypes for collagen IV. However, WT and $dy^{W-/-}$ collagen IV staining (**Figure 3.2**A-A''' and B-B''', respectively) showed no obvious differences. Collagen IV seems to be lining all myofibers (magenta asterisks) in tissue sections from both genotypes (**Figure 3.2**A'' and A''' and B'' and B''', yellow arrows).

We next used a polyclonal antibody against laminin which recognizes all laminins present in skeletal muscles. This pan-laminin antibody (**Figure 3.2**C-C''' and D-D''') shows the close relationship between muscle laminins and the myofibers (**Figure 3.2**C''-C''' and D''-D''', magenta asterisks), a pattern very similar to the one observed for collagen IV. The pan-laminin staining (**Figure 3.2**C'' and D'', yellow arrows) is identical across genotypes, most likely because laminin-411 and -511 are present in $dy^{W-/-}$ muscles[19] and are detected with the pan-laminin antibody. We then used an antibody that specifically recognizes the laminin α2 chain. As expected, laminin α2 staining is only detected in the WT fetuses (**Figure 3.2**E'', yellow arrows) and the $dy^{W-/-}$ shows no staining (**Figure 3.2**F''). In the WT sections, the pattern of laminin α2 staining is very similar to the one of pan-laminin (**Figure 3.2**C'', yellow arrows), showing that this molecule closely involves the myofibers stained with MHC (**Figure 3.2**E'' and E''', magenta asterisks).

We conclude that the absence of laminin-211 in $dy^{W-/-}$ fetuses seems to affect fibronectin deposition, as assessed by the immunohistochemistry results that we obtained. Although we attempted to address the distribution of other ECM proteins, such as perlecan, collagen I and VI, we were not able to obtain results, due to technical constraints. This should be done in the future to get a fuller picture of the ECM composition in $dy^{W-/-}$ muscles.

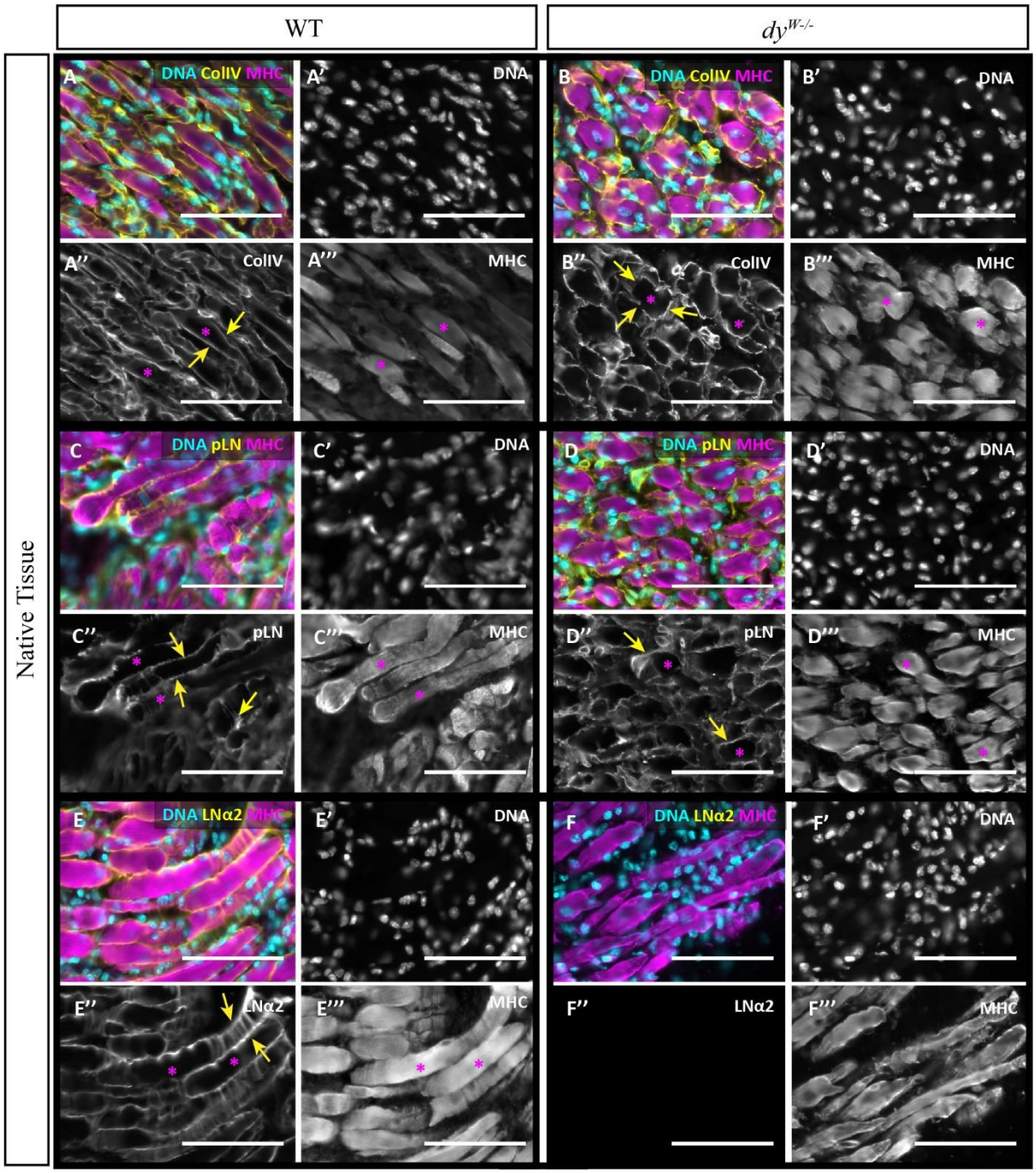

Figure 3. 2 - Characterization of the distribution of collagen IV, pan-laminin and laminin α2 in WT and *dy*$^{W-/-}$ E18.5 mouse fetuses deep back muscles. Cryosections of NT from WT and *dy*$^{W-/-}$ E18.5 fetuses processed for immunofluorescence. Immunostaining for collagen IV (ColIV) (**A** and **B**, yellow; **A''** and **B''**, grayscale), pan-laminin (pLN) (**C** and **D**, yellow; **C''** and **D''**, grayscale), laminin α2 (**E** and **F**, yellow; **E''** and **F''**, grayscale), myosin heavy chain (MHC) (**A**, **B**, **C**, **D**, **E, F**, magenta; **A'''**, **B'''**, **C'''**, **D'''**, **E'''**, **F'''**, grayscale) and DNA (**A**, **B**, **C**, **D**, **E**, **F**, cyan; **A'**, **B'**, **C'**, **D'**, **E'**, **F'**, grayscale). Magenta asterisks correspond to the same myofibers (**A''** and **A'''**, **B''** and **B'''**, **C''** and **C'''**, **D''** and **D'''**, **E''** and **E'''**). The color image (**A**, **B**, **C**, **D**, **E**, **F**) is a merge of the respective grayscale channels. Arrows and asterisks represent staining of interest with the same color. Scale bars: 75µm.

To quantify the proteins of the ECM, we performed WB analysis in WT and *dy*$^{W-/-}$ E18.5 fetuses. Protein lysates were extracted from native tissue (NT) samples of both genotypes, run in an acrylamide gel, transferred to an activated PVDF membrane and stained with several antibodies against ECM proteins of both the BM and the IM. After being developed, the membranes were then stained with Ponceau red that was quantified in each lane and served as loading control to calculate the relative ratio for all proteins. In this way, we could evaluate the relative concentration of these molecules in both genotypes. These ratios were then compared (**Annex III – Table S2**, **S3**).

Laminin α2 bands (~400 kDa) (**Figure 3.3**A) are present in both genotypes. Although not expressing a functional laminin-211, *dy*$^{W-/-}$ mice still produce a low quantity of a non-functional truncated version of α2 chain[36] that is detected by WB, reason why this lower band was much lighter than the WT counterpart. The intensity of the bands in the WT is as expected much higher than in the *dy*$^{W-/-}$ (**Figure 3.3**C, p-value=0,024).

The profile detected by the pan-laminin antibody (~200-400 kDa) is also more intense in the WT (**Figure 3.3**A). As stated before, the antibody used in this case recognizes all known laminins in skeletal muscle, which means that it is also staining laminin α2. The clear increase in intensity, when compared to laminin α2 bands, is most likely the result of the detection of a broader spectrum of laminins. *dy*$^{W-/-}$ fetuses show a much lower relative ratio than the WT (**Figure 3.3**D, p-value=0,018), representing a reduction of approximately 60%.

Regarding the proteins of the IM, fibronectin bands (220 kDa) in the WT seem more intense than in the *dy*$^{W-/-}$ fetuses (**Figure 3.3**B), even though the difference is not statistically significant (**Figure 3.3**E, p-value=0,122).

Collagen VI bands (140-150 kDa) display a similar intensity in both genotypes (**Figure 3.3**B), which is confirmed by comparing the relative ratios (**Figure 3.3**F, p-value=0,228). However, the molecular weight of this molecule seems to be altered in the *dy*$^{W-/-}$.

Interestingly, the collagen I bands (120 kDa) are more intense in the *dy*$^{W-/-}$ fetuses than in the WT (**Figure 3.3**B) and the pixel density ratio of the bands is significantly different between genotypes (**Figure 3.3**G, p-value=0,0002). Collagen I concentration is much higher in the *dy*$^{W-/-}$ fetuses than the WT, representing an almost 3-fold increase. It was not possible to detect all the proteins tested by immunohistochemistry in WB experiments due to lack of appropriate antibody availability.

There is sparse information regarding the molecular constitution of the ECM in *dy*$^{W-/-}$ mice during fetal stages. More information on these stages of development could give a better understanding of the onset of MDC1A and its consequences. Being a quantitative method, WB analysis can add value to the immunohistochemical study, and in this case, we have shown that when laminin α2 is not present in the ECM of the skeletal muscle, the presence of other proteins can be affected. These data suggest that the composition of the ECM is altered in the *dy*$^{W-/-}$ fetuses.

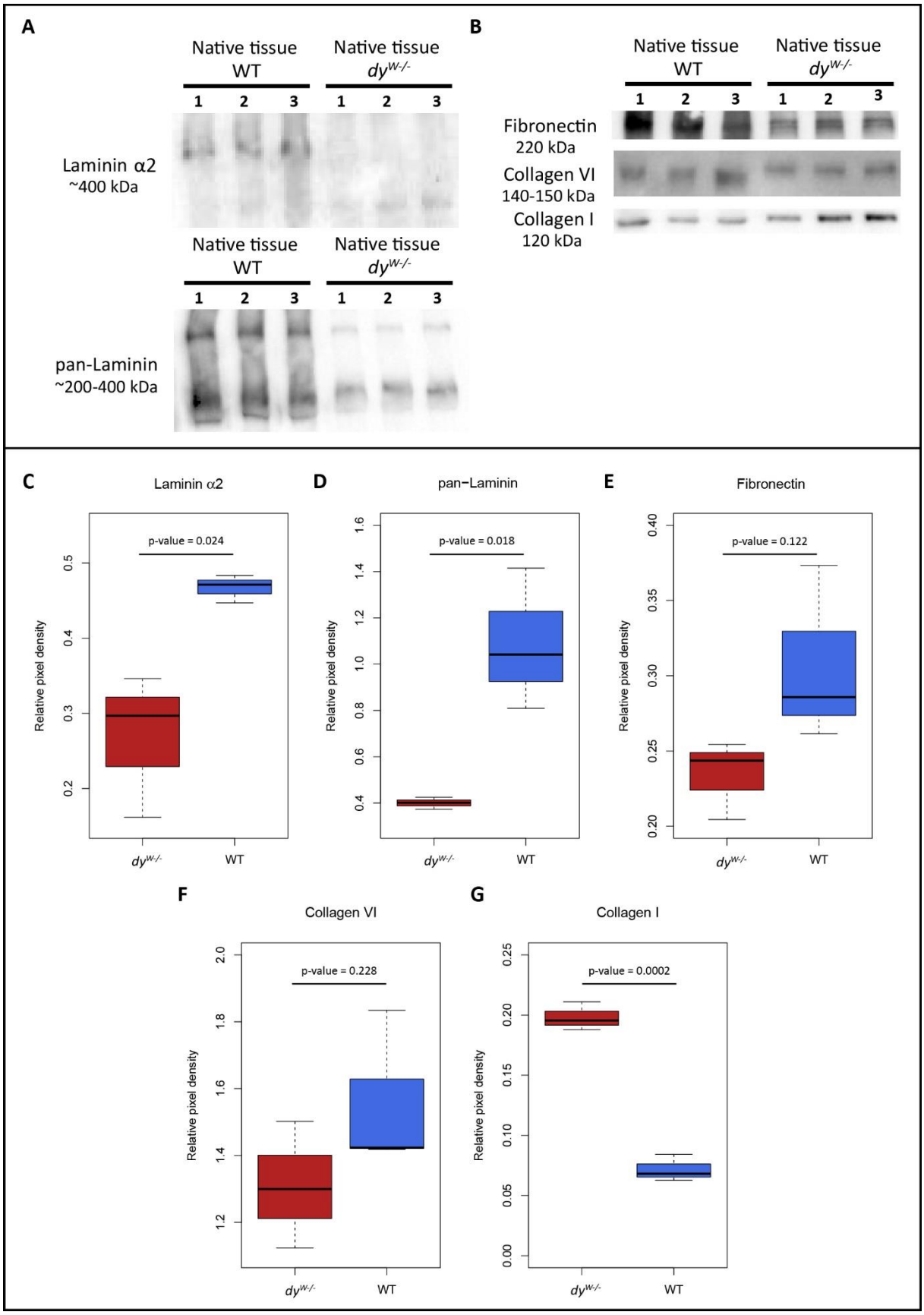

Figure 3. 3 – Western Blot analysis and relative quantification of NT ECM proteins in WT and *dy*$^{W-/-}$ E18.5 mouse fetuses. Band pattern of BMs proteins laminin α2 and pan-laminin (**A**) and IM proteins, fibronectin, collagen VI, and collagen I (**B**). **(Continues next page)**

(Continued from previous page) WT (blue) and *dy*$^{W-/-}$ (red) NT ECM proteins were extracted and separated by SDS-PAGE, blotted and immunostained with the previously mentioned antibodies (N=3 each). Bands were detected in all fetuses. Graphical representation of the relative ratio of the blotted proteins and the profile of Ponceau red staining in each lane (**C**, **D**, **E**, **F**, **G**) for laminin α2 (**C**), pan-laminin (**D**), fibronectin (**E**), collagen VI (**F**) and collagen I (**G**). Relative values are arbitrary units.

To assess if this difference has an impact on the morphology of myofibers, we processed NT from both genotypes for scanning electron microscopy (SEM) and evaluated the general appearance of the muscle. Myofibers of WT fetuses have an organized appearance and a consistent pattern of closely aligned cells (**Figure 3.4**A, white dashed line), contrasting with the *dy*$^{W-/-}$ (**Figure 3.4**B, white dashed lines) where myofibers do not always have a regular orientation and look less cohesive.

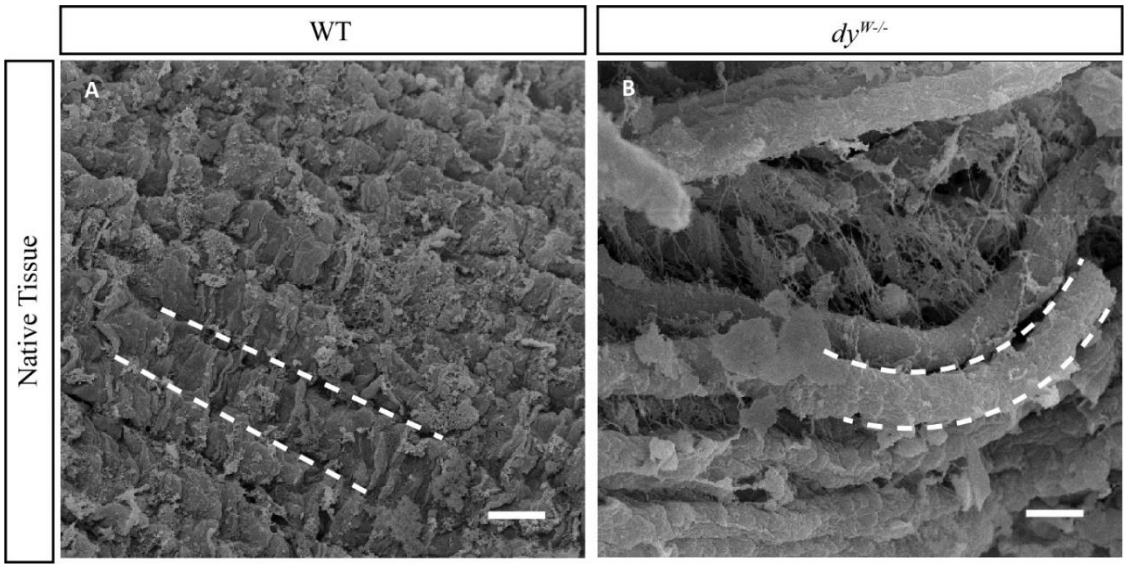

Figure 3. 4 – Scanning electron microscopy images of NT in WT and *dy*$^{W-/-}$ E18.5 mouse fetuses. WT fetal muscle (**A**) shows a more organized ECM surrounding the myofibers (white dashed line). Myofibers are aligned and show a consistent pattern. In the *dy*$^{W-/-}$ (**B**), myofibers (white dashed line) have a barer appearance suggesting a poorer ECM. Myofibers in the *dy*$^{W-/-}$ seem more disorganized and less anchored to the ECM. Scale bars: 10μm.

Regarding the ECM appearance, myofibers in the WT seem enveloped in a denser ECM than those of the *dy*$^{W-/-}$. The ECM surrounding the *dy*$^{W-/-}$ myofibers is less dense, giving them a barer appearance, which could result in their less cohesive pattern.

Decellularized fetal matrices maintain a similar ECM composition to their native tissue counterpart

In a healthy individual, laminin-211 is already present in the skeletal muscle niche when the MuSCs enter their niche[19]. However, according to recent unpublished data of our group, MuSCs also express the genes required to produce laminin-211, potentially secreting it into their niche and thus actively participating in the formation of their niche. To understand the contribution of the source of laminin-211 for the normal development of the muscle, an experimental setup that allows to dissect the specific contribution of each one of these sources was designed. Silva et al.[44] decellularized fetal cardiac tissue and demonstrated its ability to sustain fetal cardiomyocyte proliferation. Using this study as a basis, we set out to decellularize fetal deep back muscle (skeletal muscle) isolated from E18.5 WT and $dy^{W-/-}$ fetuses. Our long-term objective was to create an experimental setup where only one source (cells or ECM) of laminin-211 is present, using decellularized muscle matrices and isolated MuSCs from WT and $dy^{W-/-}$ fetuses.

We began by adapting and optimizing the protocol established by Silva et al.[44] for skeletal muscle. Our goal was to obtain a natural matrix as similar to the NT as possible in its composition but without cells. The maintenance of laminin-211 in the WT matrices was particularly important to be able to obtain a better understanding of the influence of the environment in the context of MDC1A.

NT samples (deep back muscle) of WT E18.5 fetuses were processed for decellularization. The protocol consisted of successive washes in solutions with a composition that removes all cell content (DNA and cytoplasmic proteins) from the matrices. NT samples were washed in a hypotonic buffer, which caused cell lysis and then with a detergent to remove cell membranes and other lipidic molecules. Finally, a DNase treatment was applied to degrade DNA and facilitate its removal. These 3 steps were the same in the subsequent experimental setups, where we varied the detergent step to assess which method was optimal for our material.

We started by testing a 0,2% SDS solution in the detergent step (**Figure 3.5**B-B’’’). Pilot studies in our lab had already shown that at this concentration SDS preserved some proteins of the ECM. This experimental condition originated dECMs with very low cell content. DNA (**Figure 3.5**B’) and F-actin (**Figure 3.5**B’’’) were not present. However, this process also removed laminin α2, as detected by immunostaining (**Figure 3.5**B’’). Due to the necessity of maintaining this molecule in the dECMs, we tried other detergent protocols. A lower concentration of SDS (0,05%, **Figure 3.5**C-C’’’) and 2 different concentrations of Triton X-100 (0,2% and 0,5%, **Figure 3.5**D-D’’’ and E-E’’’, respectively) were compared regarding the cell content and the preservation of laminin α2 by immunohistochemistry after decellularization.

When Triton X-100 solutions were used the resulting matrices for both conditions showed staining for laminin α2 (**Figure 3.5**D’’ and E’’, yellow arrows) and pan-laminin (**Figure 3.5**D’’’and E’’’), but the remaining cell content in these matrices was considerable (**Figure 3.5**D’ and E’, showing high-intensity staining spots in cyan circles). These results show that Triton X-100 solutions perform poorly when compared with SDS.

In the next step, we evaluated the reduction of the concentration of SDS. At a lower concentration (0,05%) SDS performs better when compared with the other conditions. Laminin α2 was preserved in the ECM of the dECMs (**Figure 3.5**C’’), showing a similar staining pattern to the NT (**Figure 3.5**A’’), delineating the space once occupied by the myofibers and the immunostaining for cell content was much lower than with the Triton X-100 solutions. DNA (**Figure 3.5**C’) and F-actin (**Figure 3.5**C’’’) staining is residual and no nuclei or myofibers were observed.

The best compromise was to keep laminin α2 even though some cell debris persisted in the dECMs. Harsher treatments (0,2% SDS) showed better elimination of these residues but also washed-out laminin α2. The presence of this protein in the dECMs was a mandatory condition in our study to approach the interactions of cells with their niche during the development of the skeletal muscle. Therefore, 0,05% SDS concentration showed the best results and was selected for the subsequent experimental setups.

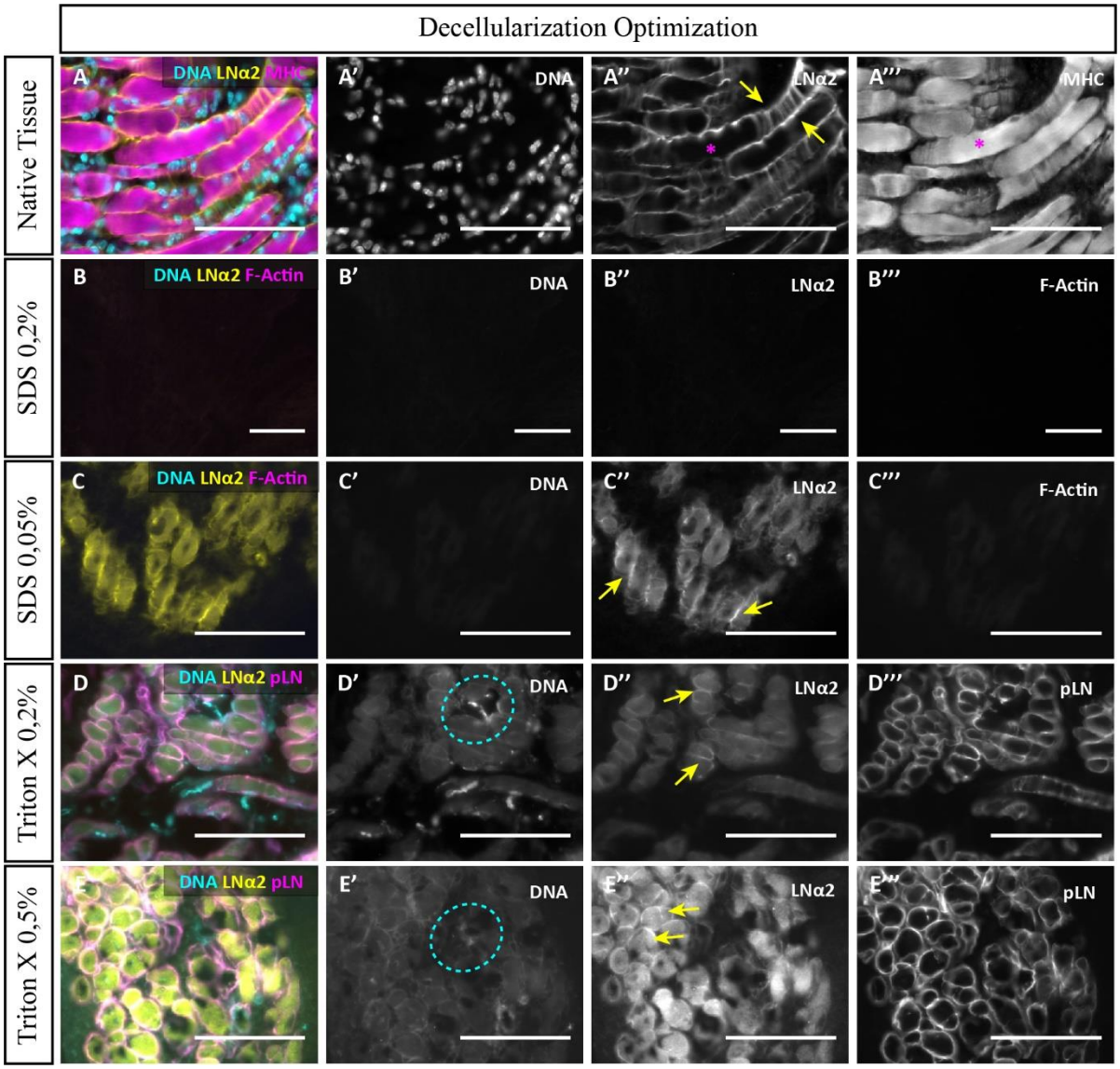

Figure 3. 5 – Different experimental conditions used during the decellularization optimization process in E18.5 WT fetuses. Cryosections of NT and dECMs of WT E18.5 fetuses processed for immunofluorescence. Immunostaining for DNA (**A**, **B**, **C**, **D**, **E**, cyan; **A'**, **B'**, **C'**, **D'**, **E'**, grayscale), laminin α2 (LNα2) (**A**, **B**, **C**, **D**, **E**, yellow; **A''**, **B''**, **C''**, **D''**, **E''**, grayscale), myosin heavy chain (MHC) (**A**, magenta; **A'''**, grayscale), f-actin (**B**, **C**, magenta; **B'''**, **C'''**, grayscale) and pan-laminin (pLN) (**D** and **E**, magenta; **D'''** and **E'''**, grayscale). The color image (**A**, **B**, **C**, **D**, **E**) is a merge of the respective grayscale channels. WT NT was submitted to successive washes in a hypotonic buffer, a detergent and a DNase treatment. All 3 steps were common on the different approaches using distinct detergent solutions (**B-B'''**, **C-C'''**, **D-D'''** and **E-E'''**). Laminin α2 staining pattern in the NT (**A'**, yellow arrows) served as control for the experimental conditions. Arrows, asterisks and circles represent staining of interest with the same color. Scale bars: 75 µm.

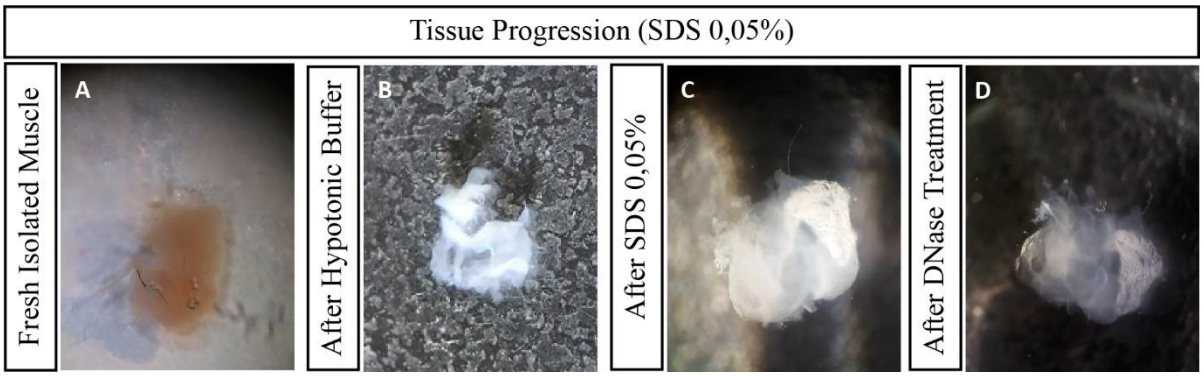

Figure 3. 6 – Tissue changes across the protocol. As the NT samples progress in the decellularization protocol (**A-D**), the changes in the appearance are noticeable. Samples start with a pinkish color, characteristic of muscle, and progressively begin to show a more transparent appearance as DNA and cell contents are washed. Laminin α2 preservation in the ECM and the minimal possible cell content was the key factor for the selection of 0.05% SDS solution for future decellularization procedures.

Throughout the protocol, the NT appearance changes progressively (**Figure 3.6**A-D). Freshly isolated muscle masses have a pinkish color characteristic of this tissue. After the hypotonic buffer incubation step, myofibers present in the muscle lyse and the myoglobin is washed away, resulting in a tissue with a much whiter appearance. After SDS and DNase treatment, these muscle masses become successively more transparent, because of the progressive removal of cell material. In the end, a transparent matrix free of cells and retaining laminin α2 is produced.

After the decellularization protocol was optimized for skeletal muscle and consistently produced matrices that maintain laminin α2 in the WT and show low cell content, we initiated the characterization of these matrices by immunohistochemistry. The same proteins selected for the characterization of the ECM of the NT were tested in these new dECMs (WT and $dy^{W-/-}$) to analyze if these matrices reliably preserved the same proteins as the NT.

As shown below, laminin α2 staining is still detected in WT dECMs (**Figure 3.7**A') and, as expected, similarly to what happens in the NT, is not present in the $dy^{W-/-}$ ones (**Figure 3.8**A'). In WT, laminin α2 staining is localized surrounding the space where myofibers were present. In both genotypes (**Figure 3.7** (WT) and **Figure 3.8** ($dy^{W-/-}$)), pan-laminin (**Figure 3.7**B' and **Figure 3.8**B', yellow arrows) and collagen IV (**Figure 3.7**C' and **Figure 3.8**C', yellow arrows) surround this same space left by the myofibers. Staining for these BM proteins is similar in both dECMs and the NT, even though there is a reduction in the intensity of the staining (**Figure 3.7** (WT) and **Figure 3.8** ($dy^{W-/-}$) in the dECMs, as compared to the NT depicted in the inserts).

In WT and $dy^{W-/-}$ dECMs, fibronectin labeling (**Figure 3.7**E'' and **Figure 3.8**D', yellow arrows, respectively) appears to be present in the same pattern as in the NT. Tenascin (**Figure 3.7**D' and **Figure 3.8**E', yellow arrows, WT and $dy^{W-/-}$, respectively) is still present, although as is the case for fibronectin, the staining is more diffuse than in the NT. These IM proteins are kept in the dECMs, however, as observed before, a decrease in the intensity of the staining seems to occur.

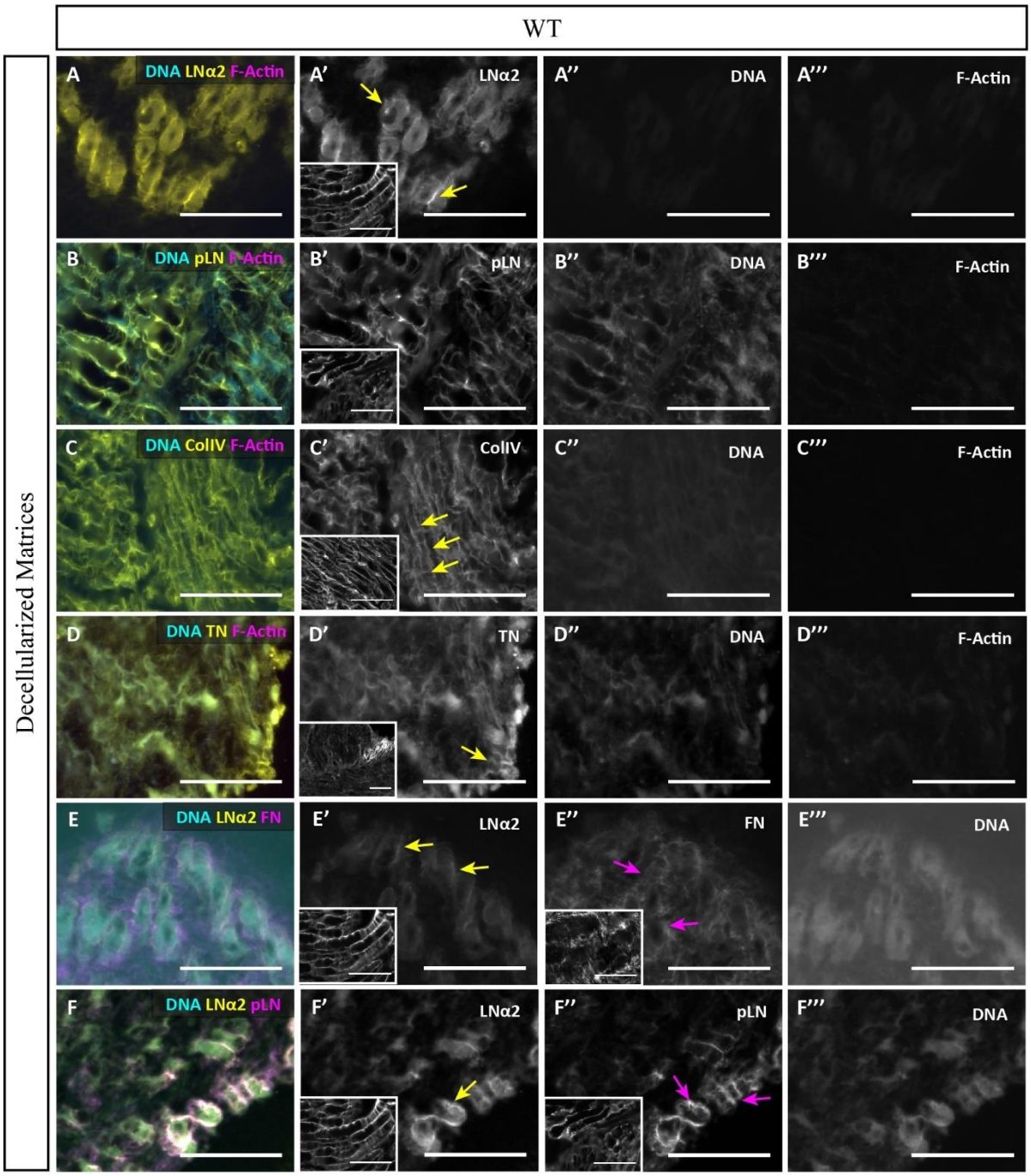

Figure 3. 7 – Characterization of the preserved ECM proteins in E18.5 WT mouse fetuses deep back muscles dECMs. Cryosections of E18.5 WT dECMs. Immunostaining for laminin α2 (LNα2) (**A**, **E** and **F**, yellow; **A'**, **E'** and **F'**, grayscale), pan-laminin (pLN) (**B** and **F**, yellow and magenta, respectively; **B'** and **F''**, grayscale), collagen IV (ColIV) (**C**, yellow; **C'**, grayscale), tenascin (TN) (**D**, yellow; **D'**, grayscale), fibronectin (FN) (**E**, magenta; **E''**, grayscale), DNA (**A**, **B**, **C**, **D**, **E**, **F**, cyan; **A''**, **B''**, **C''**, **D''**, **E'''**, **F'''**, grayscale) and f-actin (**A**, **B**, **C**, **D**, magenta; **A'''**, **B'''**, **C'''**, **D'''**, grayscale). The color image (**A**, **B**, **C**, **D**, **E**, **F**) is a merge of the respective grayscale channels. All inserts correspond to the respective protein staining in the NT (**A'**, **B'**, **C'**, **D'**, **E'** and **E''**, **F'** and **F''**). Arrows represent staining of interest with the same color. Scale bars: 75µm.

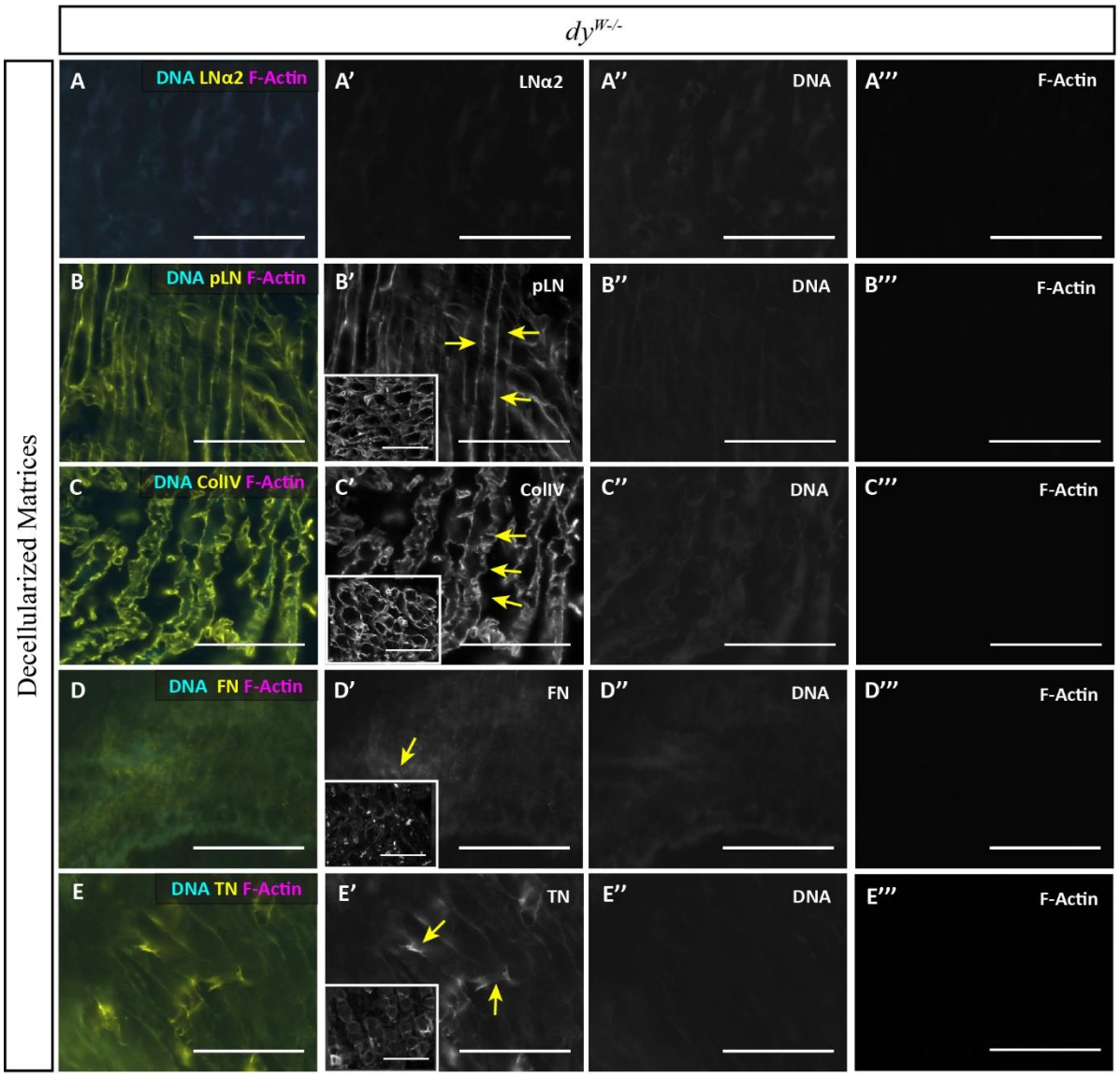

Figure 3. 8 - Characterization of the preserved ECM proteins in E18.5 *dy*$^{W-/-}$ mouse fetuses deep back muscles dECM. Cryosections of E18.5 dy$^{W-/-}$ dECMs. Immunostaining for laminin α2 (LNα2) (**A**, yellow; A', grayscale), pan-laminin (pLN) (**B**, yellow; **B'**, grayscale), collagen IV (ColIV) (**C**, yellow; **C'**, grayscale), fibronectin (FN) (**D**, yellow; **D'**, grayscale), tenascin (TN) (**E**, magenta; **E'**, grayscale), DNA (**A**, **B**, **C**, **D**, **E**, **F**, cyan; **A''**, **B''**, **C''**, **D''**, **E''**, **F''**, grayscale) and f-actin (**A**, **B**, **C**, **D**, **E**, magenta; **A'''**, **B'''**, **C'''**, **D'''**, **E'''**, grayscale). The color image (**A**, **B**, **C**, **D**, **E**) is a merge of the respective grayscale channels. All inserts correspond to the respective protein staining in the NT (**B'**, **C'**, **D'**, **E'**). Arrows represent staining of interest with the same color. Scale bars: 75 µm.

DNA (**Figure 3.7**A''-D'', E''', F''' and **Figure 3.8**A''-F'') and F-actin (**Figure 3.7**A'''-D''' and **Figure 3.8**A'''-E''') are not present in the preparations and the residual staining is neglectable.

Altogether, these results suggest that, although all the proteins tested in the dECMs are preserved, their staining intensity is lower. The decellularization protocol allows for the maintenance of the ECM proteins but as cells are washed, proteins seem to be removed to some extent.

To get a better insight of the degree of this reduction, a WB analysis of the dECMs (WT and *dy*$^{W-/-}$) ECM proteins was performed. However, due to technical difficulties in obtaining a profile of Ponceau red staining in the membrane, relative quantification was not possible.

Pan-laminin bands (**Figure 3.9**A) were detected in both genotypes and with a similar intensity. However, these bands show much lower intensity than the control (NT samples).

In the WB analysis of the ECM proteins of the NT samples, WT samples displayed bands with stronger intensity than the *dy*$^{W-/-}$ (see **Figure 3.3**A). Although laminin α2 was detected by immunohistochemistry, it was not detected in the WB experiments. This protein was already shown to have weaker bands than pan-laminin in the NT and after decellularization, it was no longer detected in the present analysis. These results indicate that likely there is a reduction of laminins after decellularization.

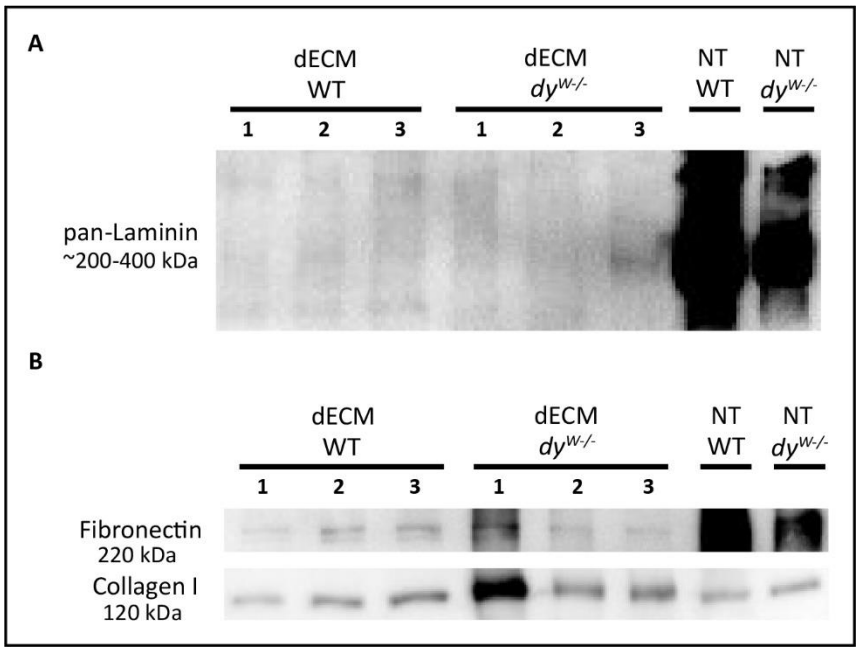

Figure 3. 9 - Western Blot analysis of ECM proteins present in WT and *dy*$^{W-/-}$ dECMs. Band pattern of BMs protein pan-laminin (**A**) and IM proteins, fibronectin and collagen I (**B**). dECMs and NT (control) ECM proteins were extracted and separated by SDS-PAGE, blotted and immunostained with the previously mentioned antibodies (N=3 each). Bands were detected in all fetuses.

Fibronectin bands (**Figure 3.9**B) were detected in fetal muscle of both genotypes, with higher intensity in the WT samples (except for fetus 1 of each genotype). The NT bands showed a similar result. This protein followed the same trend as pan-laminin, with lower band intensity in the decellularized samples. Collagen I bands (**Figure 3.9**B) were stronger in the *dy*$^{W-/-}$, again following the same pattern as in NT (except for fetus 1 in both genotypes). Collagen VI was not detected in the dECMs (data not shown).

The decellularization protocol may introduce some artifacts that affect the quantification of the concentration of the protein lysates, resulting in under- or over-loading of proteins in the gels. This is observed in fetus 1 of both genotypes (**Figure 3.9**B). This error can also be the reason behind the lower intensity of the bands of collagen I of the NT when compared to the decellularized counterpart.

Following the same approach as in NT, we then characterized the morphology of the dECMs (WT and *dy*$^{W-/-}$) by SEM. SEM images show that both dECMs (WT and *dy*$^{W-/-}$, **Figure 3.10**A and B, respectively) are very similar: there are no myofibers present and the matrices adopt an amorphous appearance when compared to NT (inserts). This result shows that the decellularization protocol successfully eliminates myofibers, although the ECM network is more amorphous in dECMs than in NT.

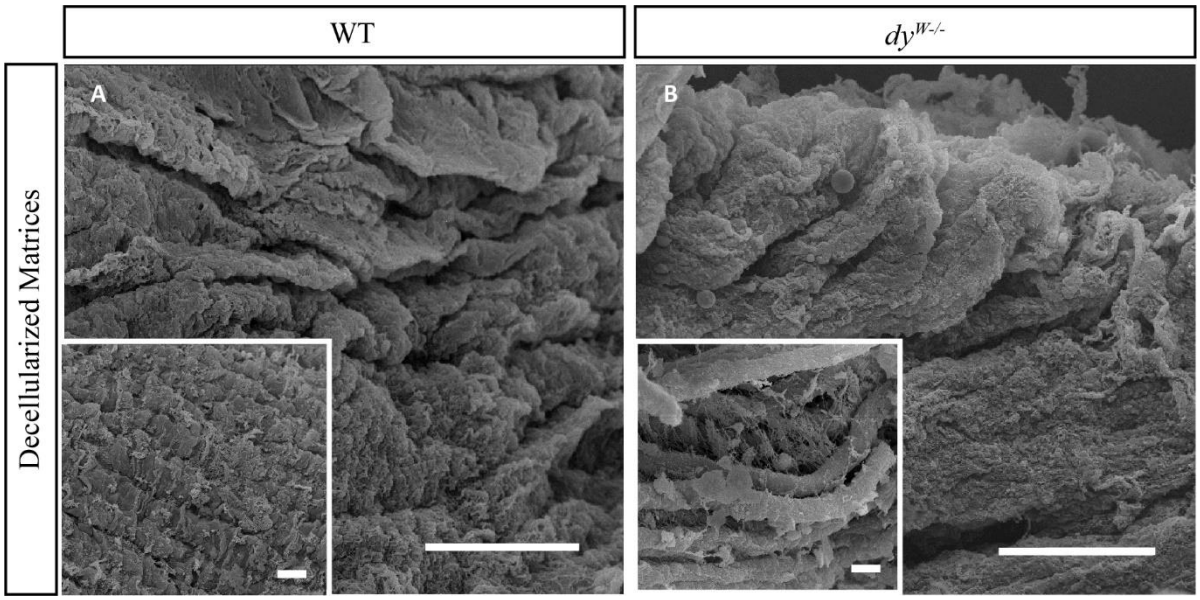

Figure 3. 10 – Scanning electron microscopy images of WT and *dy*$^{W-/-}$ E18.5 dECMs. WT dECMs (**A**) have a similar appearance to dy$^{W-/-}$ (**B**). Both genotypes show no organized myofibers and a more amorphous appearance when compared to the NT (see inserts). The decellularization protocol is effective in the elimination of myofibers. Scale bars: 50 μm and 10 μm in the inserts.

Decellularized matrices can support and sustain cells and are remodeled by their presence

The decellularization protocol was efficient, producing dECMs with a similar composition to their native counterparts (with some reduction in protein quantity). The objective of the decellularization was to create a model that would allow to experimentally study the two sources of laminin-211 (that produced by MuSCs versus the ECM already present when they enter their niche) and by doing this to understand the contribution of each source for the correct development of the muscle. These matrices seem to maintain laminin α2 in their composition as shown in the immunohistochemistry analysis.

As a next step, we seeded muscle cells into dECMs and compared their behavior in the presence (WT matrices) or absence (*dy*$^{W-/-}$ matrices) of laminin α2. We began by cultivating these matrices with cryopreserved MuSCs isolated from fetal muscles, although these cells failed to adhere/expand (data not shown).

We next used C2C12 cells, which are an established adult skeletal muscle stem cell line (satellite cells) and have the advantage of being more resistant while maintaining their stem cell proprieties, and therefore represent a good alternative model to the fetal MuSCs. It was previously shown in our group that these cells produce laminin α2 (unpublished data).

The cultures were successful and the dECMs of fetal muscle from both genotypes were colonized by C2C12 cells. Two timepoints were established during the cell culture experiments: 8 days and 15 days after cell seeding. All the results are obtained from the 8 days timepoint, because as time progressed the matrices showed signs of degradation and decreased cell viability (data not shown).

C2C12 cells are able to infiltrate the matrices and appear to preferentially occupy the space left by the removed myofibers (data not shown). Moreover, these cells display aligned nuclei and acquire a fusiform shape, signs of possible differentiation into myotubes (**Figure 3.11**A and B, white asterisks).

The presence of these cells completely changes the shape of the dECMs. The controls without cells (**Figure 3.11**C) show a less compact shape when compared to the ones seeded with C2C12 cells (**Figure 3.11**D). These cells seem to be able to contract the matrix, giving it a more rounded appearance.

To assess if the presence or absence of laminin α2 affected the ability of C2C12 cells to colonize and proliferate in the dECMs we compared the number of cells present in the matrices of each genotype. The number of cells, although not significantly different (p-value= 0.055, **Annex IV – Table S5**), suggests that cells tend to infiltrate or proliferate better in the WT dECMs (containing laminin α2). For the same area, $dy^{W-/-}$ matrices support on average around 142 cells while the WT matrices have an average of close to 205 cells. An increase in sample size (N) could allow us to verify if this observed difference is indeed statistically significant (**Figure 3.11**E).

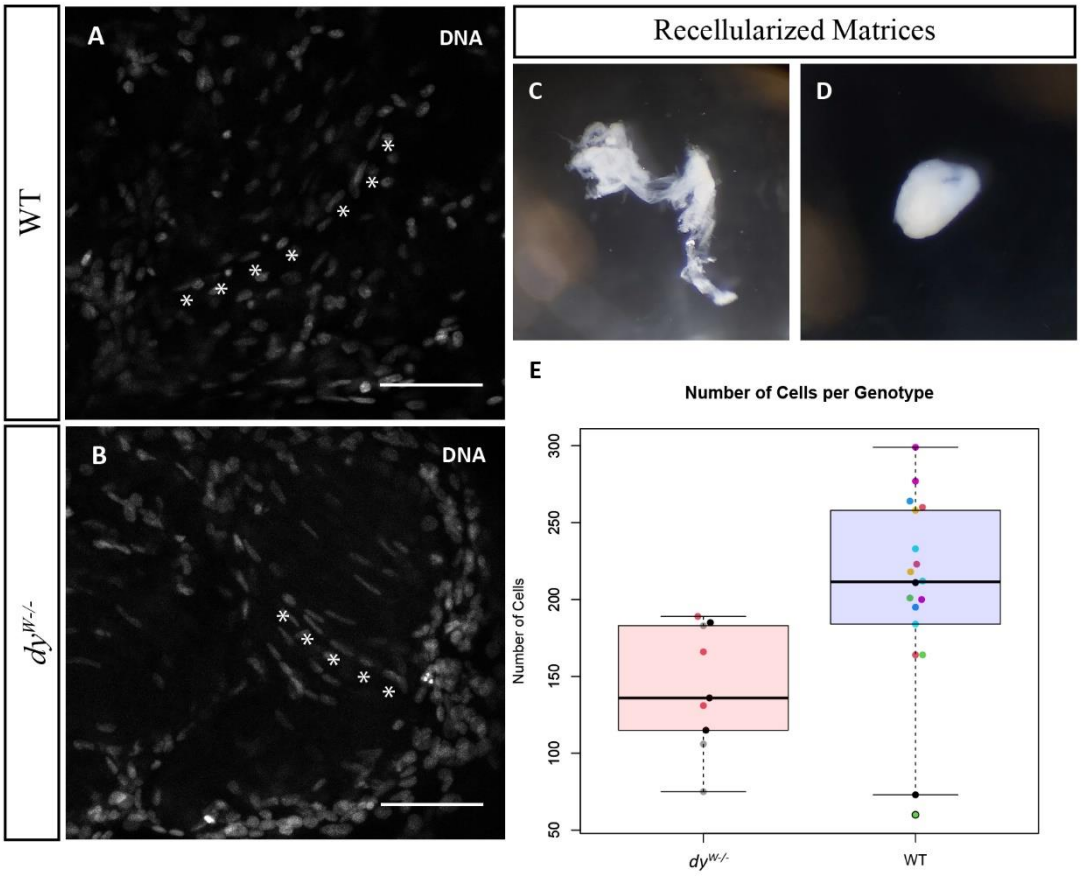

Figure 3. 11 – Decellularized WT and $dy^{W-/-}$ matrices seeded with C2C12 cells. dECMs without cells (control) (**A**) and seeded with C2C12 cells (**B**) show a distinct shape, the latter one displaying a rounder appearance. *In toto* confocal optical sections of WT and $dy^{W-/-}$ dECMs (**C**, **C'** and **D**, **D'**, respectively). Staining for DNA (**C**, **D**, grayscale). These images show that C2C12 cells infiltrate the matrices, start to align and acquire a more fusiform shape (white asterisks) in both genotypes (**C** (WT) and **D** ($dy^{W-/-}$)). These images also suggest that WT dECMs tend to have more cells than the $dy^{W-/-}$ ones. To assess if this statement was true C2C12 cells were counted in matrices of both genotypes (WT, N=7; $dy^{W-/-}$, N=3). Graphical representation of this data (area measured: 180x180μm) (**E**) shows that, although not statistically significant (p=0,055), there is a tendency for the presence of more cells in the WT (blue) than in the $dy^{W-/-}$ (pink). Each color point represents the replicates of an individual matrix. Scale bar: 100 μm.

These results show that dECMs of both genotypes can sustain C2C12 cells, that attach and survive, and provide them with the necessary conditions for these cells to differentiate and fuse, as suggested by the images obtained showing nuclear alignment.

To clarify if these cells are actively producing ECM proteins, secreting and assembling them, immunohistochemistry was performed in the recellularized matrices (WT and *dy*$^{W-/-}$, **Figure 3.12)**. Laminin α2 staining surrounding these cells is present in the recellularized matrices of both genotypes (**Figure 3.12**C'', yellow arrows (WT) and **Figure 3.12**E'', yellow arrow (*dy*$^{W-/-}$)). Intracellular staining is also present (**Figure 3.12**B'-B''', yellow arrows near the red asterisk (WT) and **Figure 3.12**F'-F'', yellow arrows near the cyan asterisk (*dy*$^{W-/-}$)).

In the WT matrices, pan-laminin staining was observed around cells (**Figure 3.12**B''', magenta arrow near the cyan asterisk) but also in their interior (**Figure 3.12**B' and B''', magenta arrow near the red asterisk), following a pattern like that observed for laminin α2. The same staining pattern was observed in the *dy*$^{W-/-}$ (**Figure 3.12**E''', uppermost magenta arrow (interior of cells) and in the same image, the below magenta arrow (exterior)).

Finally, fibronectin was detected in the spaces between cells (WT, **Figure 3.12**D''', the below magenta arrows and the *dy*$^{W-/-}$, **Figure 3.12**F''', leftmost magenta arrow) but some intracellular staining (WT, **Figure 3.12**D''', upmost magenta arrow and in the *dy*$^{W-/-}$, **Figure 3.12**F' and F''', magenta arrows near the red asterisk) was also observed in both genotypes. Localization of other ECM proteins was attempted but was not successful due to technical difficulties.

Altogether, these results suggest that C2C12 cells that colonized these matrices are not only using the matrices as a scaffold but actively producing new ECM proteins and remodeling their niche.

Although time was short to obtain more results, this culture system model, ideally used for the culture of native MuSCs isolated from fetal muscles, seems promising for studying the exact contribution of laminin-211 in the native ECM versus that produced by MuSCs in shaping their niche as well as its effects on their proliferation and differentiation.

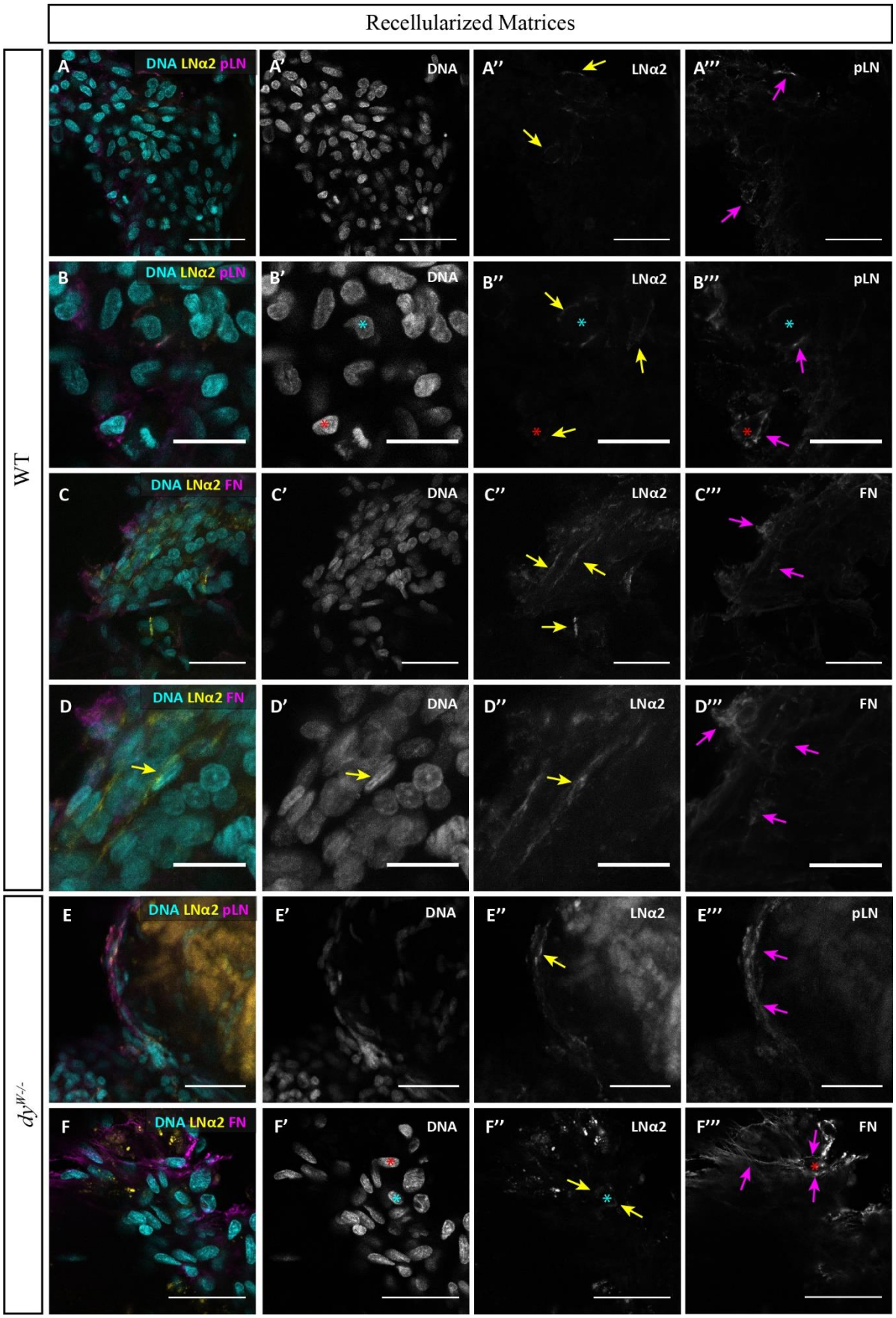

Figure 3. 12 - Characterization of the ECM proteins produced by C2C12 cells in WT and $dy^{W-/-}$ dECMs. Sections of WT and $dy^{W-/-}$ dECMs (**A-A'''**, **B-B'''**, **C-C'''** and, **D-D'''** and **E-E'''**, respectively). **(Continues next page)**

(Continued from previous page) Immunostaining for laminin α2 (LNα2) (**A**, **B**, **C**, **D**, **E**, **F**, yellow; **A''**, **B''**, **C''**, **D''**, **E''**, **F''** grayscale), pan-laminin (pLN) (**A**, **B**, **E**, magenta; **A'''**, **B'''**, **E'''**, grayscale), fibronectin (FN) (**C**, **D**, **F**, magenta; **C'''**, **D'''**, **F'''** grayscale), and DNA (**A**, **B**, **C**, **D**, **E**, **F**, cyan; **A'**, **B'**, **C'**, **D'**, **E'**, **F'**, grayscale). The color image (**A**, **B**, **C**, **D**, **E**, **F**) is a merge of the respective grayscale channels. Arrows and asterisks represent staining of interest with the same color. Scale bar: 75μm (**A**, **C**, **E**, **F**) and 25μm (**B**, **D**).

CHAPTER 4
DISCUSSION

Discussion

ECM composition differs in both genotypes

Most information about MDC1A is from postnatal observations[55] and there is an extreme need for a more detailed understanding of the molecular and cellular effects of laminin α2 deficiency during development. Therefore, further investigation is needed to unveil the process involved in the regulation of MuSC by laminin-211. Our group showed that the onset of MDC1A in the mouse occurs *in utero* and seems to be due to an abnormal depletion of the MuSC pool between E17.5 and E18.5. The mechanism behind this regulation is still unknown[19].

In this work, we characterized some of the major molecules of the fetal muscle ECM in the $dy^{W-/-}$ mouse model in comparison with WT. Immunohistochemistry results show that both genotypes show similar levels of protein staining for the majority of the proteins under study. However, fibronectin seems reduced in $dy^{W-/-}$ (**Figure 3.1**B) and the expected laminin α2 is absent. WB analysis was also performed for the same proteins (except tenascin and collagen IV due to technical impossibility).

Interestingly, the same trend observed in immunohistochemistry was detected in fibronectin band intensity in the WB analysis (**Figure 3.3**B). Although not statistically significant, $dy^{W-/-}$ displays lighter bands of fibronectin. These results suggest that fibronectin production in $dy^{W-/-}$ *f*etuses seems to be lower than in WT. MDC1A is characterized by chronic inflammation and fibrosis of the skeletal muscle. However, these symptoms were only observed in postnatal and adult tissue[56]. Fibronectin deposition is described in the fibrotic tissue postnatally[57]. Our results suggest that in the fetus the trend seems to be actually the opposite.

Another considerable difference between $dy^{W-/-}$ and WT fetuses was the 3-fold increase in collagen I production in $dy^{W-/-}$ (**Figure 3.3**B, G). Unfortunately, collagen I could not be tested in immunohistochemistry due to technical constraints and therefore its localization was not assessed. Collagen I production is associated with inflammatory processes, a major symptom of MDC1A[56,58]. This could indicate that this symptom, although not morphologically observed, starts to emerge already during development and not just after birth. Fibronectin is known to promote myoblast migration and fusion *in vitro*[10] and loss of this protein in the MuSCs ECM has been reported to impair muscle regeneration in the adult[59]. Fibronectin regulates symmetric divisions of MuSCs and knockdown experiments show a decreased ability to repopulate their niche[60]. Collagen I and fibronectin production is regulated by the transforming growth factor (TGF)-β pathway[60,61] which has already been described as upregulated postnatally in MDC1A[62]. Further analysis of TGF- β expression and downstream pathways in fetal muscle could help discern this dichotomy of upregulated collagen I and downregulated fibronectin during these early stages. Collagen I upregulation is associated with regenerative processes[61]. Together, these results may suggest that in the absence of laminin-211 and in a fibronectin deficient environment myofibers may promote an increase in collagen I production to buffer the defective myofiber growth. Further analysis is needed to address if the fetal stages recapitulate the adult. Phosphorylated STAT3 (pSTAT3) is upregulated in $dy^{W-/-}$ postnatally and seems to be also increased in fetal stages (although not statistically significant). A simultaneous increase in pSTAT3 and myostatin is associated with aged muscle leading to loss of regeneration capacity[19]. The same is true for loss of fibronectin in the MuSCs niche[59]. This is consistent with the reduced regeneration potential of $dy^{W-/-}$ muscles[19].

Residual bands were detected in $dy^{W-/-}$ fetuses when staining for laminin α2. This fact has been described in this model mice which still produce a truncated unfunctional α2 chain of laminins[36] (**Figure 3.3**A). Laminins also seems to suffer a decrease of 60% in $dy^{W-/-}$(**Figure 3.3**A, D). No reports of other

laminins' decrease are described. Controversially, the opposite has been observed. *LAMA4* overexpression was detected in MDC1A patients[63] and compensation with laminin-411 and -511 was also described[37]. These proteins are inadequate compensators and are not able to recover the defect[37]. The decrease in pan-laminin bands intensity in $dy^{W-/-}$ could be due to the absence of laminin α2 that is not being detected and therefore contributing to lower band intensity or another possible explanation could be that the absence of this protein could be altering other laminins expression. Further analysis of specific isoforms could clarify this question.

Collagen VI is another molecule that showed differences between genotypes (**Figure 3.3**B). This protein deposition has been observed to be increased postnatally in dystrophic mice[55]. Our results show similar band intensities in both genotypes but collagen VI appears to have a slightly different molecular weight in $dy^{W-/-}$, suggesting that the absence of laminin α2 may induce (or prevent) some type of post-translational modification that alters this molecule. Mutations that affect post-translational modifications of collagens (lysyl hydroxylase) have been described to originate other pathologies, such as Ehlers-Danlos syndrome that manifest similar symptoms to MDC1A[64].

Altogether, these results suggest that the absence of laminin-211 affects at least some other ECM proteins in $dy^{W-/-}$muscles. Another indication of changes in ECM composition comes from the SEM images obtained in this study, where $dy^{W-/-}$ muscle fibers seem barer and smoother in appearance than WT fibers (**Figure 3.4**). Previous studies in our lab revealed that $dy^{W-/-}$ fetuses have smaller myofibers when compared with the WT[19]. The SEM images add new data concerning the ECM surrounding these myofibers contributing to a better understanding of this microenvironment.

Decellularization efficiently removes cell content and preserves ECM proteins

Silva et al.[44] decellularized neonatal cardiac tissue and successfully colonized it with fetal cardiomyocytes. These migrated toward the center of the scaffold and displayed elongated morphology and excellent viability, showing that dECMs can help to achieve therapeutic approaches[44].

As previously stated, when MuSCs start entering their niche under the myofiber BM at E16.5, the myofibers are already surrounded by an ECM containing laminin-211. MuSCs are also able to produce laminin-211 and potentially secrete it to their niche. Having this in mind, we aimed to create a model that allows to study separately each one of these sources of laminin-211. Decellularization of native skeletal muscle tissue (WT and $dy^{W-/-}$) allowed to produce a matrix that would, or not, have laminin-211 in its composition. We compared different approaches to the decellularization process. The original protocol was optimized to fetal cardiac tissue, which is denser, so we had to adapt it to fetal skeletal muscle. The main goal of decellularization was to remove the cell content and keep an ECM composition similar to that of the NT. We concluded that using a 0.05% SDS solution provided better results (**Figure 3.5**C). A compromise between the presence of cell debris and laminin α2 preservation was adopted. Triton X-100 is a weaker detergent when compared to SDS and has been shown that the latter seems more effective in removing cellular content in denser tissues while preserving tissue mechanics[65]. However, this detergent has some cytotoxicity and ECM ultrastructure disruption as a drawback[41]. After decellularization, no myofibers are detected and dECM acquire an amorphous appearance (**Figure 3.10**).

Decellularization of skeletal muscle is a relatively new method of producing scaffolds for skeletal muscle engineering. The first to develop a multi-step process of decellularization was Carlson et al.[66] in 1991. Since this, great advances have occurred. The majority of studies on decellularized skeletal muscle were made in adults and focused on regeneration[67–69]. We believe that with the present study,

for the first time, a protocol of decellularization for fetal skeletal muscle was established and, in this case, in the context of MDC1A.

After the protocol was established, we assessed how ECM proteins were affected by the decellularization. Immunohistochemistry showed that the tested proteins are preserved in the dECMs but a decrease in staining intensity is detected (**Figure 3.7** and **Figure 3.8**). The WB analysis confirmed these data (**Figure 3.9**). A decrease in protein quantity in dECMs has been described even when using mild decellularization techniques[70]. An important step to make the use of the bioscaffolds in clinics more reliable is the correct quantification and characterization of the proteins in the dECMs. Techniques such as quantitative proteomics can allow the precise comparison between different decellularization protocols and their refinement[71].

Interestingly, the trend observed in the NT is maintained in the dECMs: lower levels of fibronectin and higher levels of collagen I in $dy^{W-/-}$ (**Figure 3.9**B). Laminin α2 bands in WB were no longer detected after the decellularization in both genotypes. The obtained bands by WB on the NT were already very faint in both genotypes and, after decellularization, disappeared After decellularization, laminin α2 is detected in the WT in immunohistochemistry but not in WB. Pan-laminin antibody in WB showed a big reduction on the band intensity (when compared to the NT) after decellularization, although it was still detectable in both genotypes (**Figure 3.9**A). This difference could be the result of the process of decellularization generating artifacts in the lysates of the dECMs that affect protein quantification leading to protein under loading (**Figure 3.9**B**,** $dy^{W-/-}$ dECM: fetus 1). The use of a more precise quantification method should resolve this problem.

C2C12 cells colonize and remodel the decellularized matrices

Our results show that C2C12 cells have the ability to infiltrate and align but also contract the dECMs (**Figure 3.11**A-B and D, respectively). C2C12 myoblasts fuse with each other during differentiation to form myotubes *in vitro*[10]. A hallmark of differentiation in C2C12 myoblasts is the alignment of these cells and the presence of fusiform nuclei[72], suggesting that these cells are showing signs of differentiation. Analysis of myogenic regulatory factors, such as Myo-D, myogenin or MHC staining, could have helped to clarify the differentiation status of the C2C12 cells within the dECMs if time had allowed[73].

In this work, we seeded decellularized fetal matrices with C2C12 myoblasts as an alternative to native fetal myoblasts or MuSCs. The latter would give more reliable information about the *in vivo* processes. However, due to their difficulty of isolation, low yield number and sensitivity to experimental conditions, C2C12 myoblasts were used. These cells are an immortalized line originated from mice post-injury adult satellite cells that are widely used as a skeletal muscle culture model[54,73,74]. Many decellularization studies have used this cell line with great success[68,75,76].

As previously stated, the ultimate goal of this work was to study each one of the components that act as sources of laminin-211. Our results suggest that in the presence of laminin-211, C2C12 cells tend to proliferate or infiltrate more in the matrices when compared to laminin-211 deficient matrices (although the difference did not reach statistical significance with our sample size). The dissection of these two processes should be further analyzed in future dedicated experiments. The presence of laminin-211 has been shown to promote faster spreading of C2C12 cells[77]. This indicates that C2C12 cells take advantage of a substrate that has laminin-211, even if able to produce this protein autonomously. The ability to colonize $dy^{W-/-}$ dECMs could be due to the presence of other adhesion molecules such as fibronectin, collagen IV or other laminins present in the substrate. These cells may also use their own

capacity to produce laminin-211 to compensate for its absence. Further analysis of these factors could help discern these hypotheses.

Diverse experimental therapies to ameliorate MDC1A are ongoing. Supplementation with laminin-111[78] or CRISPR/Cas9 editing of the *LAMA2* gene[79] in dystrophic mice models of MDC1A are showing some positive results in reverting this disease to some extent. A similar gene-editing approach in pig and human models of Duchenne muscular dystrophy (lack of dystrophin) had great success in ameliorating this disease and paves the way to a possible application to MDC1A[80]. Our results suggest that C2C12 cells are actively producing other ECM proteins, such as laminins and fibronectin, thus contributing to the construction of their niche (**Figure 3.12**). This opens the possibility for normal cells to participate, at least in part, in the recovery of a defective niche. In MDC1A, MuSCs fail to expand due to the absence of laminin-211[19,36] and, maybe in the future, it would be possible that cell therapies could revert this defect. MDC1A prevalence and the inexistence of any effective treatment highlights the urgency in gaining a deeper understanding of the mechanisms behind this disease. Detailed knowledge of the dynamics involved in skeletal muscle development could allow the targeting of key events and prevent this condition.

Further perspectives

We established, for the first time, a decellularization model (**Figure 4.1**) that allows to study both sources of laminin-211 (ECM and cells). In the future, MuSCs isolation and culture conditions fine-tuning will be needed to accurately understand the relative contribution of each source. Plans to generate a C2C12 *LAMA2*-knockout line are ongoing in our lab, which could constitute another alternative to MuSCs. When the model is fully optimized for MuSCs, we will be able to seed dECMs and test cell behavior within and across genotypes. The results will tell the relative contribution of each source of laminin-211 for the correct development of skeletal muscle. This work represents a new approach to unveil the developmental dynamics behind MDC1A. Contributions of this model can lead to a better understanding of this disease and, hopefully in the future, help mitigate this devastating illness.

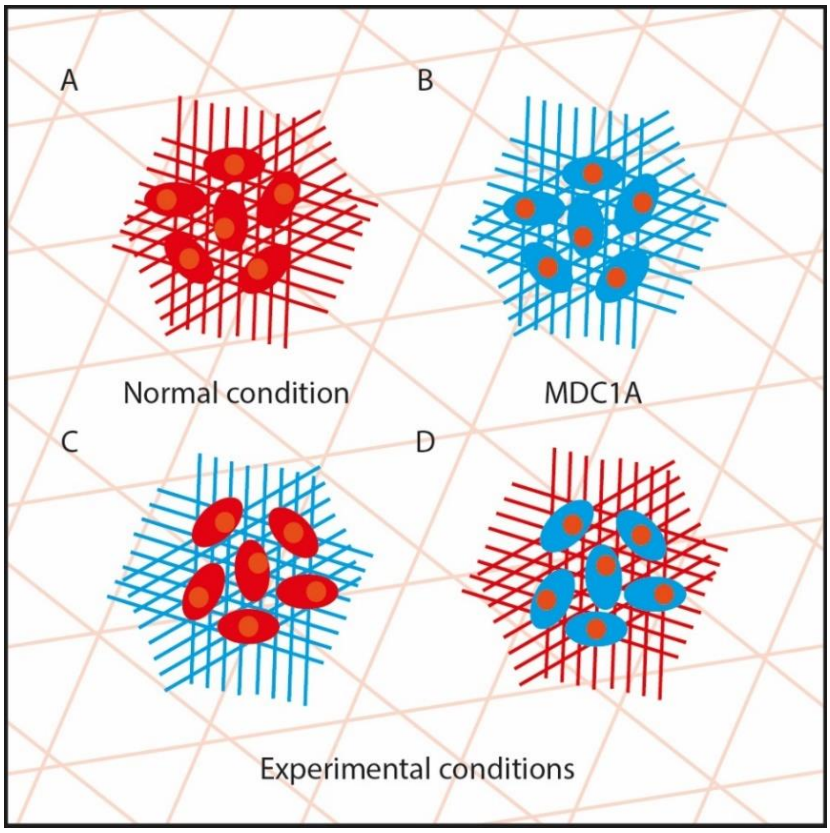

Figure 4. 1 – The model developed in the group. In normal skeletal muscle development, laminin-211 is present in the matrix and is produced by MuSCs (**A**). When laminin-211 is not present, muscle development is impaired, developing MDC1A (**B**) Laminin-211 producing MuSCs (red cells) can be seed in mutant dECMs (blue grid) (**C**) and mutant cells (blue cells) in normal dECMs (red grid) (**D**).

CHAPTER 5
BIBLIOGRAPHY

Bibliography

1. Mecham, R. P. Overview of Extracellular Matrix. *Curr. Protoc. Cell Biol.* **57**, 10.1.1-10.1.16 (2012).

2. Özbek, S., Balasubramanian, P. G., Chiquet-Ehrismann, R., Tucker, R. P. & Adams, J. C. The evolution of extracellular matrix. *Mol. Biol. Cell* **21**, 4300–4305 (2010).

3. Frantz, C., Stewart, K. M. & Weaver, V. M. The extracellular matrix at a glance. *Journal of Cell Science* **123**, 4195–4200 (2010).

4. Rozario, T. & DeSimone, D. W. The extracellular matrix in development and morphogenesis: A dynamic view. *Developmental Biology* **341**, 126–140 (2010).

5. Mallet, D. G. & Pettet, G. J. A mathematical model of integrin-mediated haptotactic cell migration. *Bull. Math. Biol.* **68**, 231–253 (2006).

6. King, S. J. *et al.* Lamellipodia are crucial for haptotactic sensing and response. *J. Cell Sci.* **129**, 2329–2342 (2016).

7. Lucero, H. A. & Kagan, H. M. Lysyl oxidase: An oxidative enzyme and effector of cell function. *Cellular and Molecular Life Sciences* **63**, 2304–2316 (2006).

8. Thorsteinsdóttir, S., Deries, M., Cachaço, A. S. & Bajanca, F. The extracellular matrix dimension of skeletal muscle development. *Developmental Biology* **354**, 191–207 (2011).

9. Laurila, P. & Leivo, I. Basement membrane and interstitial matrix components form separate matrices in heterokaryons of PYS-2 cells and fibroblasts. *J. Cell Sci.* **104**, 59–68 (1993).

10. Vaz, R., Martins, G. G., Thorsteinsdóttir, S. & Rodrigues, G. Fibronectin promotes migration, alignment and fusion in an in vitro myoblast cell model. *Cell Tissue Res.* **348**, 569–578 (2012).

11. Giblin, S. P. & Midwood, K. S. Tenascin-C: Form versus function. *Cell Adhesion and Migration* **9**, 48–82 (2015).

12. Bedini, E., Corsaro, M. M., Fernández-Mayoralas, A. & Iadonisi, A. Chondroitin, Dermatan, Heparan, and Keratan Sulfate: Structure and Functions. in *Extracellular Sugar-Based Biopolymers Matrices* 187–233 (2019).

13. Rifes, P. & Thorsteinsdóttir, S. Extracellular matrix assembly and 3D organization during paraxial mesoderm development in the chick embryo. *Dev. Biol.* **368**, 370–381 (2012).

14. Thorsteinsdóttir, S. Basement membrane and fibronectin matrix are distinct entities in the developing mouse blastocyst. *Anat. Rec.* **232**, 141–149 (1992).

15. Yurchenco, P. D. Integrating Activities of Laminins that Drive Basement Membrane Assembly and Function. *Curr. Top. Membr.* **76**, 1–30 (2015).

16. LeBleu, V. S., MacDonald, B. & Kalluri, R. Structure and Function of Basement Membranes. *Exp. Biol. Med.* **232**, 1121–1129 (2007).

17. Walma, D. A. C. & Yamada, K. M. The extracellular matrix in development. *Development (Cambridge, England)* **147**, (2020).

18. Deries, M. & Thorsteinsdóttir, S. Axial and limb muscle development: dialogue with the neighbourhood. *Cellular and Molecular Life Sciences* **73**, 4415–4431 (2016).

19. Nunes, A. M. *et al.* Impaired fetal muscle development and JAK-STAT activation mark disease onset and progression in a mouse model for merosin-deficient congenital muscular dystrophy. *Hum. Mol. Genet.* **26**, 2018–2033 (2017).

20. Bajanca, F. *et al.* Integrin α6β1-laminin interactions regulate early myotome formation in the mouse embryo. *Development* **133**, 1635–1644 (2006).

21. Relaix, F., Rocancourt, D., Mansouri, A. & Buckingham, M. A Pax3/Pax7-dependent population of skeletal muscle progenitor cells. *Nature* **435**, 948–953 (2005).

22. Kjær, M. Role of Extracellular Matrix in Adaptation of Tendon and Skeletal Muscle to Mechanical Loading. *Physiological Reviews* **84**, 649–698 (2004).

23. Buckingham, M. & Rigby, P. W. J. Gene Regulatory Networks and Transcriptional Mechanisms that Control Myogenesis. *Developmental Cell* **28**, 225–238 (2014).

24. Sanes, J. R. The basement membrane/basal lamina of skeletal muscle. *Journal of Biological Chemistry* **278**, 12601–12604 (2003).

25. Deries, M., Schweitzer, R. & Duxson, M. J. Developmental fate of the mammalian myotome. *Dev. Dyn.* **239**, 2898–2910 (2010).

26. Deries, M. *et al.* Extracellular matrix remodeling accompanies axial muscle development and morphogenesis in the mouse. *Dev. Dyn.* **241**, 350–364 (2012).

27. Patton, B. L., Miner, J. H., Chiu, A. Y. & Sanes, J. R. Distribution and function of laminins in the neuromuscular system of developing, adult, and mutant mice. *J. Cell Biol.* **139**, 1507–1521 (1997).

28. Biressi, S., Molinaro, M. & Cossu, G. Cellular heterogeneity during vertebrate skeletal muscle development. *Developmental Biology* **308**, 281–293 (2007).

29. Wigmore, P. M. & Evans, D. J. R. Molecular and cellular mechanisms involved in the generation of fiber diversity during myogenesis. *Int. Rev. Cytol.* **216**, 175–232 (2002).

30. Zammit, P. S. & Beauchamp, J. R. The skeletal muscle satellite cell: Stem cell or son of stem cell? *Differentiation* **68**, 193–204 (2001).

31. Lamandé, S. R. & Bateman, J. F. Genetic Disorders of the Extracellular Matrix. *Anat. Rec.* **303**, 1527–1542 (2020).

32. Lovering, R. M., Porter, N. C. & Block, R. J. The muscular dystrophies: From genes to therapies. *Physical Therapy* **85**, 1372–1388 (2005).

33. Mendell, J. R., Boué, D. R. & Martin, P. T. The congenital muscular dystrophies: Recent advances and molecular insights. *Pediatric and Developmental Pathology* **9**, 427–443 (2006).

34. Theocharis, A. D., Manou, D. & Karamanos, N. K. The extracellular matrix as a multitasking player in disease. *FEBS Journal* **286**, 2830–2869 (2019).

35. Tome, F. M. S. *et al.* Congenital muscular dystrophy with merosin deficiency. *Comptes Rendus l'Academie des Sci. - Ser. III* **317**, 351–357 (1994).

36. Gawlik, K. I. & Durbeej, M. Skeletal muscle laminin and MDC1A: pathogenesis and treatment strategies. *Skeletal Muscle* **1**, 9 (2011).

37. Yurchenco, P. D., Crosson, S., McKee, K. K. & Ruegg, M. A. M.I.1 Mechanism of laminin assembly: Insight for structural repairs of MDC1A. *Neuromuscul. Disord.* **23**, 738 (2013).

38. Nelson, I. *et al.* Laminin α2 Deficiency-Related Muscular Dystrophy Mimicking Emery-Dreifuss and Collagen VI related Diseases. *J. Neuromuscul. Dis.* **2**, 229–240 (2015).

39. Allamand, V. & Guicheney, P. Merosin-deficient congenital muscular dystrophy, autosomal recessive (MDC1A, MIM#156225, LAMA2 gene coding for α2 chain of laminin). *Eur. J. Hum. Genet.* **10**, 91–94 (2002).

40. Kuang, S., Kuroda, K., Le Grand, F. & Rudnicki, M. A. Asymmetric Self-Renewal and Commitment of Satellite Stem Cells in Muscle. *Cell* **129**, 999–1010 (2007).

41. Crapo, P. M., Gilbert, T. W. & Badylak, S. F. An overview of tissue and whole organ decellularization processes. *Biomaterials* **32**, 3233–3243 (2011).

42. McCrary, M. W., Bousalis, D., Mobini, S., Song, Y. H. & Schmidt, C. E. Decellularized tissues as platforms for in vitro modeling of healthy and diseased tissues. *Acta Biomaterialia* **111**, 1–19 (2020).

43. Koh, I. *et al.* The mode and dynamics of glioblastoma cell invasion into a decellularized tissue-derived extracellular matrix-based three-dimensional tumor model. *Sci. Rep.* **8**, 1–12 (2018).

44. Silva, A. C. *et al.* Three-dimensional scaffolds of fetal decellularized hearts exhibit enhanced potential to support cardiac cells in comparison to the adult. *Biomaterials* **104**, 52–64 (2016).

45. Fedecostante, M. *et al.* Recellularized native kidney scaffolds as a novel tool in nephrotoxicity screening s. *Drug Metab. Dispos.* **46**, 1338–1350 (2018).

46. Wagner, D. E. *et al.* Comparative decellularization and recellularization of normal versus emphysematous human lungs. *Biomaterials* **35**, 3281–3297 (2014).

47. Wassenaar, J. W., Boss, G. R. & Christman, K. L. Decellularized skeletal muscle as an invitro model for studying drug-extracellular matrix interactions. *Biomaterials* **64**, 108–114 (2015).

48. Brouki Milan, P. *et al.* Decellularization and preservation of human skin: A platform for tissue engineering and reconstructive surgery. *Methods* **171**, 62–67 (2020).

49. Chen, W. C. W. *et al.* Decellularized zebrafish cardiac extracellular matrix induces mammalian heart regeneration. *Sci. Adv.* **2**, (2016).

50. Gilbert, T. W. Strategies for tissue and organ decellularization. *J. Cell. Biochem.* **113**, 2217–2222 (2012).

51. Kuang, W. *et al.* Merosin-deficient congenital muscular dystrophy: Partial genetic correction in two mouse models. *J. Clin. Invest.* **102**, 844–852 (1998).

52. Truett, G. E. *et al.* Preparation of PCR-quality mouse genomic dna with hot sodium hydroxide and tris (HotSHOT). *Biotechniques* **29**, 52–54 (2000).

53. Bajanca, F., Luz, M., Duxson, M. J. & Thorsteinsdóttir, S. Integrins in the mouse myotome: Developmental changes and differences between the epaxial and hypaxial lineage. *Dev. Dyn.* **231**, 402–415 (2004).

54. Yaffe, D. & Saxel, O. Serial passaging and differentiation of myogenic cells isolated from

dystrophic mouse muscle. *Nature* **270**, 725–727 (1977).

55. Durbeej, M. Laminin-α2 Chain-Deficient Congenital Muscular Dystrophy. Pathophysiology and Development of Treatment. *Curr. Top. Membr.* **76**, 31–60 (2015).

56. Gawlik, K. I., Körner, Z., Oliveira, B. M. & Durbeej, M. Early skeletal muscle pathology and disease progress in the dy 3K /dy 3K mouse model of congenital muscular dystrophy with laminin α2 chain-deficiency. *Sci. Rep.* **9**, 1–17 (2019).

57. Mehuron, T. *et al.* Dysregulation of matricellular proteins is an early signature of pathology in laminin-deficient muscular dystrophy. *Skelet. Muscle* **4**, (2014).

58. Alexakis, C., Partridge, T. & Bou-Gharios, G. Implication of the satellite cell in dystrophic muscle fibrosis: a self-perpetuating mechanism of collagen overproduction. *Am. J. Physiol. Physiol.* **293**, C661–C669 (2007).

59. Lukjanenko, L. *et al.* Loss of fibronectin from the aged stem cell niche affects the regenerative capacity of skeletal muscle in mice. *Nat. Med.* **22**, 897–905 (2016).

60. Bentzinger, C. F. *et al.* Fibronectin regulates Wnt7a signaling and satellite cell expansion. *Cell Stem Cell* **12**, 75–87 (2013).

61. Hillege, M. *et al.* TGF-β Regulates Collagen Type I Expression in Myoblasts and Myotubes via Transient Ctgf and Fgf-2 Expression. *Cells* **9**, 375 (2020).

62. Gawlik, K. I. *et al.* Potent pro-inflammatory and profibrotic molecules, osteopontin and galectin-3, are not major disease modulators of laminin α2 chaindeficient muscular dystrophy. *Sci. Rep.* **7**, (2017).

63. Kölbel, H. *et al.* Identification of candidate protein markers in skeletal muscle of laminin-211-deficient CMD type 1A-patients. *Front. Neurol.* **10**, 470 (2019).

64. Yamauchi, M. & Sricholpech, M. Lysine post-translational modifications of collagen. *Essays Biochem.* **52**, 113–133 (2012).

65. Nakayama, K. H., Batchelder, C. A., Lee, C. I. & Tarantal, A. F. Decellularized rhesus monkey kidney as a three-dimensional scaffold for renal tissue engineering. *Tissue Eng. - Part A* **16**, 2207–2216 (2010).

66. Carlson, E. C. & Carlson, B. M. A method for preparing skeletal muscle fiber basal laminae. *Anat. Rec.* **230**, 325–331 (1991).

67. Urciuolo, A. & De Coppi, P. Decellularized tissue for muscle regeneration. *International Journal of Molecular Sciences* **19**, (2018).

68. Shapiro, L. *et al.* In vitro evaluation of functionalized decellularized muscle scaffold for in situ skeletal muscle regeneration. *Biomed. Mater.* **14**, (2019).

69. McClure, M. J. *et al.* Decellularized Muscle Supports New Muscle Fibers and Improves Function Following Volumetric Injury. *Tissue Eng. - Part A* **24**, 1228–1241 (2018).

70. Calle, E. A. *et al.* Targeted proteomics effectively quantifies differences between native lung and detergent-decellularized lung extracellular matrices. *Acta Biomater.* **46**, 91–100 (2016).

71. Hill, R. C., Calle, E. A., Dzieciatkowska, M., Niklason, L. E. & Hansen, K. C. Quantification of

extracellular matrix proteins from a rat lung scaffold to provide a molecular readout for tissue engineering. *Mol. Cell. Proteomics* **14**, 961–973 (2015).

72. Rochlin, K., Yu, S., Roy, S. & Baylies, M. K. Myoblast fusion: When it takes more to make one. *Developmental Biology* **341**, 66–83 (2010).

73. Burattini, S. *et al.* C2C12 murine myoblasts as a model of skeletal muscle development: Morpho-functional characterization. *Eur. J. Histochem.* **48**, 223–233 (2004).

74. Denes, L. T. *et al.* Culturing C2C12 myotubes on micromolded gelatin hydrogels accelerates myotube maturation. *Skelet. Muscle* **9**, 1–10 (2019).

75. Perniconi, B. *et al.* Muscle acellular scaffold as a biomaterial: Effects on C2C12 cell differentiation and interaction with the murine host environment. *Front. Physiol.* **5**, (2014).

76. Wolf, M. T., Daly, K. A., Reing, J. E. & Badylak, S. F. Biologic scaffold composed of skeletal muscle extracellular matrix. *Biomaterials* **33**, 2916–2925 (2012).

77. Schuler, F. & Sorokin, L. M. Expression of laminin isoforms in mouse myogenic cells in vitro and in vivo. *J. Cell Sci.* **108**, 3795 LP – 3805 (1995).

78. Rooney, J. E., Knapp, J. R., Hodges, B. L., Wuebbles, R. D. & Burkin, D. J. Laminin-111 protein therapy reduces muscle pathology and improves viability of a mouse model of merosin-deficient congenital muscular dystrophy. *Am. J. Pathol.* **180**, 1593–1602 (2012).

79. Kemaladewi, D. U. *et al.* A mutation-independent approach for muscular dystrophy via upregulation of a modifier gene. *Nature* **572**, 125–130 (2019).

80. Moretti, A. *et al.* Somatic gene editing ameliorates skeletal and cardiac muscle failure in pig and human models of Duchenne muscular dystrophy. *Nature Medicine* **26**, 207–214 (2020).

ANNEXES

Annex I – Protocols, reagents and solutions

P1 – Genotyping

Mice tail lysis for DNA extraction

1. Cut 1-2mm tail snips and place into an Eppendorf tube.
2. Add 75ul of Buffer 1.
3. Place in thermocycler at 95ºC for 30min, cool samples to 4º C.
4. Add 75ul of Buffer 2.
5. Centrifuge at 4000rpm for 3 minutes.
6. Take an aliquot for PCR (use 1 ul undiluted).

PCR of unknown genotype DNA samples

1. Prepare the Master Mix solution (23µL per sample). Add 1µL of DNA to Master Mix.
2. Run unknown samples and a positive (heterozygous dy^W) and negative control (water) with the following PCR program:

PCR program		
95ºC	5’	
95ºC	30’’	
60.6ºC	30’’	x 35 cycles
72ºC	45’’	
72ºC	10’’	
4ºC	-	

3. Run PCR samples in a 1% agarose electrophoresis gel (agarose and TBE 0.5X) for 30min with NZYDNA Ladder V (NZYTech) at 110V and 400mA.
    a. Laminin allele wild-type band: 250bp
    b. Laminin allele LacZ mutant band: 480bp

Master Mix (1 sample)	**Buffer 1**	**Buffer 2**	**1% agarose gel**	**TBE 10x:**
GoTaq: 12.5µL **dyWFP**: 0.5µL **dyWRP**: 0.5µL **LacZ**: 0.5µL **H_2O**: 9µL **Total**: 23µL	**25mM NaOH** **0.2mM EDTA** **dH2O** until final volume	**40 mM Tris HCl** Adjust pH to 5.5	**TBE 0.5X**: 50mL **Agarose**: 0.5g **Green Safe**: 1µL	**Tris**: 53.91g **Boric Acid**: 27.52g **0.5M EDTA**: 20mL **dH2O** until 500mL

Note: dyWFP and dyWRP means dy^W Forward Primer and dy^W Reverse Primer.

P2 – Fetal skeletal muscle Decellularization

Day 1

1. Thaw the cryopreserved fetal muscle in PBS 1X (10µL of Pen/Strep for 1000µL added) in a Petri dish.
2. Wash the samples at least twice during 10-15 min in PBS 1X (10µL of Pen/Strep for 1000µL added) on ice with low agitation (60 rpm) (remove the remnants of OCT from the tissue).
3. Add 3mL of Hypotonic Buffer (10µL of Pen/Strep for 1000µL added) to each well of a 12-well plate (1 piece per well).
4. Incubate the tissue fragments overnight (18h) with Hypotonic Buffer, under agitation (165 rpm), at 25ºC.

Day 2

1. Wash the samples 3 times with PBS 1X (1 hour per wash), under agitation (165 rpm), at 25ºC.
2. Incubate the tissue 24 hours with SDS (0.02%, 0,05% and 0,2%) or Triton X-100 (0,2%, 0,5%) diluted in Hypotonic Wash Buffer solution (filtered), under agitation (165 rpm), at 25ºC.

Day 3

1. Wash the tissue fragments 3 times with Hypotonic Wash Buffer (20min per wash), under agitation (165 rpm), at 25ºC.
2. Incubate the tissue fragments during 3 hours with 2 mL of DNase treatment, under agitation (165 rpm), at 37ºC.
3. Wash the tissue fragments 3 times with PBS 1X (20min per wash), under agitation (165 rpm), at 25ºC.
4. Final wash overnight, 25ºC, 60 rpm.

PBS 10X:	**Hypotonic Wash Buffer**	**Hypotonic Buffer**	**DNase treatment**
NaCl: 137mM **KCl**: 2.68mM **Na_2HPO_4**: 8.1mM **KH_2PO_4**: 1.47mM **dH_2O** until final volume Adjust pH to 6.8	**Tris Base**: 1.21g **dH_2O**: 1L Adjust pH to 7.8	**Tris Base**: 1.21g **EDTA**: 1g **dH_2O**: 1L Adjust pH to 7.8	**Tris Base**: 1.21g **1M $MgCl_2$**: 1mL **dH_2O**: 0.5L Adjust pH to 7.8
SDS 0.2%	**Triton X-100 0.2%**		
SDS: 0.2g **Hypotonic Wash Buffer**: 100mL	**Triton X-100**: 0.2g **Hypotonic Wash Buffer**: 100mL		

P3 – Immunohistochemistry (Cryosections and *in toto*)

Embedding of samples for Cryosectioning

1. Fix samples in 4% paraformaldehyde (PFA) in 0.12M phosphate buffer with 4% sucrose (4% FISH) for at least 4h at 4ºC.
2. Wash 2 times for 10min with PBS 1X.
3. Keep overnight or over day in solution 1 (0.12M phosphate buffer with 4% sucrose) at 4ºC.
4. Wash and keep overnight or over day in solution 2 (0.12M phosphate buffer with 15% sucrose) at 4ºC. Let samples warm to room temperature.
5. Incubate for 3h in solution 3 (0.12M phosphate buffer with 15% sucrose and 7.5% gelatin) at 37ºC.
6. Make small aluminum boats and place a thin layer of fresh T3 solution and let solidify. Place the samples and cover with warm solution 3 solution. Orient the samples and let solidify. Mark location with a color pen.
7. Freeze by placing boats on the surface of dry ice-chilled or liquid nitrogen-chilled isopentane.

Cryosections Antibody Incubation

1. Mount frozen gelatin cubes containing the samples in the cryostat with O.C.T. compound (Tissue-Tek).
2. Cut the frozen gelatin cubes and transfer sections to the slides. Let sections dry for 60min.
3. Delineate samples with the hydrophobic marker.
4. Wash slides 3 times in PBS 1X (10min each).
5. Cover sections with 5% BSA diluted in PBS 1X for the blocking step for 30min.
6. Dilute the primary antibodies in 1% BSA diluted in PBS 1X and cover sections. Incubate overnight at 4ºC.
7. Wash slides 3 times (10min each) with PBS 1X.
8. Dilute the secondary antibodies in 1% BSA diluted in PBS 1X and cover sections. Incubate for 1h30min at room temperature.
9. Wash slides 3 times (10min each) with PBS 4X.
10. Submerge slides in DAPI (5µg/mL) for 30secs each.
11. Quick rinse in PBS 1X.
12. Mount preparations with anti-fading medium (50mg/ml n-propyl-gallate in PBS:glycerol (1:9)) and seal with a coverslip.

In toto Immunohistochemistry

See step 1 from “Embedding of samples for Cryosectioning” and steps 4-11 from “Cryosections Antibody Incubation”. DNA was stained with Methyl green (at the same time of the secondary antibodies) and DAPI. Samples were mounted in steel rings in-between 2 coverslips glued with beeswax.

FISH 2%	0.12M Phosphate Buffer	Anti-fading medium
Sucrose: 8g **1M $CaCl_2$**: 24µL **0.2M Na_2HPO_4**: 77mL **0.2M NaH_2PO_4**: 23mL **Paraformaldehyde**: 2g **dH2O**: until 200mL Adjust pH to 7.4	**Na_2HPO_4**: 13.5g **NaH_2PO_4**: 3.2g **dH2O**: 1L Adjust pH to 7.4	**n-Propyl-gallate**: 0,5% **PBS 10X**: 1mL **Glycerol**: 9mL
Solution 1	**Solution 2**	**Solution 3**
Sucrose: 4g **0.12M Phosphate Buffer**: 100mL	**Sucrose**: 15g **0.12M Phosphate Buffer**: 100mL	**Sucrose**: 15g **0.12M Phosphate Buffer**: 100mL **Gelatin**: 7.5g Heat at 37ºC

P4 – SEM samples preparation

1. Fix samples in 2mL of a mixture of 2.5% glutaraldehyde and 4% PFA diluted in phosphate buffer (Fixer) for 6h at 4ºC, with agitation in a hybridization tube.
2. Wash 3 times (10min each) with phosphate buffer with agitation.
3. Dehydrate through the following regimen (15min each):
    a. 30 % ethanol
    b. 50 % ethanol
    c. 70 % ethanol
    d. 80 % ethanol
    e. 90 % ethanol
    f. 100% ethanol
    g. 100% ethanol
    h. 100% ethanol
4. Transfer to a tube containing acetone until dehydration in a critical point dryer.
5. Transfer samples to a critical point dryer and dry samples.
6. Coat surface of samples with gold salts.

0.1M Phosphate Buffer	PFA 20%	Fixer
Na_2HPO_4: 12.46g **NaH_2PO_4**: 4.08g **dH2O**: 1L Adjust pH to 7.2	**Paraformaldehyde**: 20g **0.1M Phosphate Buffer**: 100mL	**PFA 20%**: 4mL **0.1M Phosphate Buffer**: 14mL **Glutaraldehyde 25%**: 2mL

P5 – Western Blot analysis

Protein extraction

1. Isolate organ/tissue from mice and immediately put it in an Eppendorf tube (2mL) containing 2X SDS-PAGE loading buffer with freshly added DTT (100mM DTT).
2. Homogenize in mixer mill for 5min using one tungsten carbide bead per tube (use chilled tube mounts).
3. Sonicate samples in an ultrasound bath for 5min (or until foam is formed).
4. Heat samples for 10min at 50ºC.
5. Centrifuge samples at 4ºC, at max speed for 15min.
6. Transfer supernatant into a fresh 1.5 mL Eppendorf tube.
7. Quantify protein using Nanodrop (Protein Abs 280nm).
8. Store at -20ºC until further use.

Polyacrylamide gel Electrophoresis

1. Mount gel cassette with 1.5mm spacers.
2. Prepare 6% and 8% Tris/Glycine SDS-Polyacrylamide electrophoresis separating gels. Fill the gel cassette with a pipette. Pour distilled (d) H_2O over the gel to ensure a flat surface. Let polymerize at room temperature. Prepare Stacking gels. Remove dH_2O. Pour the stacking gel over the solid separating gel with a pipette. Place the comb in the gel cassette. Let polymerize at room temperature. Gels composition:

Separating Gels			**Stacking Gels**
Acrylamide percentage	6%	8%	-
dH2O	5.3mL	4.6mL	2.7mL
30% Acrylamide mix	2mL	2.7mL	670µL
1.5M Tris Base (PH 8.8)	2.5mL	2.5mL	-
1M Tris Base (PH 6.8)	-	-	500µL
10% SDS	100µL	100µL	40µL
10% Ammonium Persulfate (APS)	100µL	100µL	40µL
TEMED	8µL	6µL	4µL
Total	10mL	10mL	4mL

3. Transfer the gel cassette to the electrophoresis tank containing Running Buffer 1X until the line showed in the tank (depends on the number of gels).
4. Carefully remove the comb and ensure that the wells are filled with Running Buffer. Load 50µg of protein from each sample in each well. Load 10 µL of HiMark™ Pre-stained Protein Standard (Invitrogen).
5. Run for 80min with constant voltage (10min at 150V and 70min at 175V).

Transfer

1. Soak the filter pads with chilled Transfer Buffer (4ºC).
2. Activate the PVDF membranes with methanol and rinse with dH_2O. Soak in Transfer Buffer containing 20% methanol and 0.05% SDS.

3. Mount the transfer cassette with the gels, activated membranes and filter pads.
4. Transfer the cassette to the electrophoresis tank (on a bed of ice) containing the chilled Transfer Buffer. Add the cooling unit. Run for 90min at 100V.
5. After the transfer stain with BlueSafe (NZYTech) to assess the transfer quality.

Antibody incubation and Development

1. Prepare the blocking solution (TBST with 5% milk added). Incubate the membranes with agitation for 1h.
2. Rinse 3 times with TBST.
3. Incubate the membranes overnight with the primary antibodies diluted in TBST with 5% BSA and 0.01% sodium azide (3mL for each membrane) in a cold chamber (4ºC) with agitation.
4. In the next day, wash 3 times (5min each) with TBST.
5. Incubate the membranes with HRP-conjugated secondary antibodies diluted in TBST with 5% milk (5mL for each membrane) for 1h at room temperature.
6. Wash the membranes with TBST 3 times (5min each). Keep in TBST until membrane development.
7. Use 1 mL of Detection Reagent 1 and Detection Reagent 2 of the Pierce™ ECL Western Blotting Substrate developing kit per membrane and let soak. Acquire bands images.
8. To test more than one antibody per membrane, after development, strip the former antibodies with 3 washes (5min each) with TBST and repeat step 3-7.

2X SDS-PAGE loading buffer	**TBST**	**Running Buffer 10X**	**Transfer Buffer**
Glycerol: 20% **SDS**: 4% **Tris Base**: 100 mM **Bromophenol blue**: 0.2% Adjust pH to 6.8 **DTT**: 100 mM (before use)	**Tris base**: 20mM **NaCl**: 150Mm **Tween-20**: 0.1% **dH_2O** until final volume	**Tris base**: 30.2g **Glycine**: 144.2g **SDS**: 10g **dH_2O**: 1L	**Tris base**: 5.82g **Glycine**: 2.93g **SDS**: 0.5g **Methanol**: 200mL **dH_2O** until 1L

P6 – Cell culture in decellularized matrices

1. Process the decellularized matrices and cut into pieces of approximately 500µm x 500µm x 200µm in PBS 1X with Pens/Strep (1%) added in the laminar flow hood.
2. Transfer the pieces into a 96-well plate with 200µL of DMEM with 10% FBS and 1% Pens/Strep added (complete medium) warmed to 37ºC.
3. Let soak for 2h in the incubator (37ºC and 5% CO_2).
4. Trypsinize (500µL) a T25 flask seeded with non-confluent C2C12 cells.
5. Resuspend in 1mL of complete medium and centrifugate for 5min. Remove supernatant and add 3mL of complete medium.
6. Add 10µL of complete medium with cells and 10µL trypan blue dye and load mix into the hemocytometer. Count and calculate cell number and assess cell viability.
7. Remove medium from the 96-well plate containing the decellularized matrices and add 50000 C2C12 cells diluted in 200µL of complete medium.

8. After 2 days in the incubator (37ºC and 5% CO_2), transfer the decellularized matrices (with cells) to a 48-well plate with 400µL of complete medium added. Change the medium every 2 days until the timepoint (8 or 15 days).

Annex II – Antibodies

Table S. 1 - Antibodies and respective dilutions used and their proprieties

						Immuno-histo-chemis-try	West-ern Blot
Antibody	**Clon-ality**	**Raised in**	**1º/2º**	**Manufac-turer**	**Catalog Number**	**Dilution**	
α-Fibronectin	Poly-clonal	Rabbit	Primary	Sigma	F-3648	1:500	1:5000
α-Tenascin-C	Poly-clonal	Rabbit	Primary	H. Erickson (Duke U.)	2873	1:100	-
α-Laminin α2	Mono-clonal	Rat	Primary	Sigma	L-0663	1:100	1:1000
α-pan-Laminin	Poly-clonal	Rabbit	Primary	Sigma	L- 9393	1:200	1:5000
α-Collagen I	Poly-clonal	Rabbit	Primary	abcam	ab21285	-	1:3000
α-Collagen IV	Poly-clonal	Rabbit	Primary	Millipore	AB756P	1:100	-
α-Collagen VI	Mono-clonal	Mouse	Primary	D.S.H.B.	39	1:200	1:1000
α-MHC	Mono-clonal	Mouse	Primary	D.S.H.B.	MF20	1:200	-
α-Mouse Alexa 488	Poly-clonal	Goat	Second-ary	Molecular Probes	A–11017	1:1000	-
α-Mouse Alexa 568	Poly-clonal	Goat	Second-ary	Molecular Probes	A–11019	1:1000	-
α-Rabbit Alexa 568	Poly-clonal	Goat	Second-ary	Molecular Probes	A–11070	1:1000	
α-Rabbit Alexa 568	Poly-clonal	Goat	Second-ary	Molecular Probes	A21069	1:1000	-
α-Rat Alexa 488	Poly-clonal	Goat	Second-ary	Molecular Probes	A11006	1:1000	-
Phalloidin Alexa 488	-	-	Dye	Thermo Fisher Sci.	A12379	1:200	-
Phalloidin Alexa 568	-	-	Dye	Invitrogen	A12380	1:200	-
HRP-α-Mouse IgG	Poly-clonal	Goat	Second-ary	abcam	ab205719	-	1:5000
HRP-α- Rabbit IgG	Poly-clonal	Goat	Second-ary	abcam	ab205718	-	1:5000
HRP-α- Rat IgG	Poly-clonal	Goat	Second-ary	abcam	ab205720	-	1:2500

Note: α means anti.

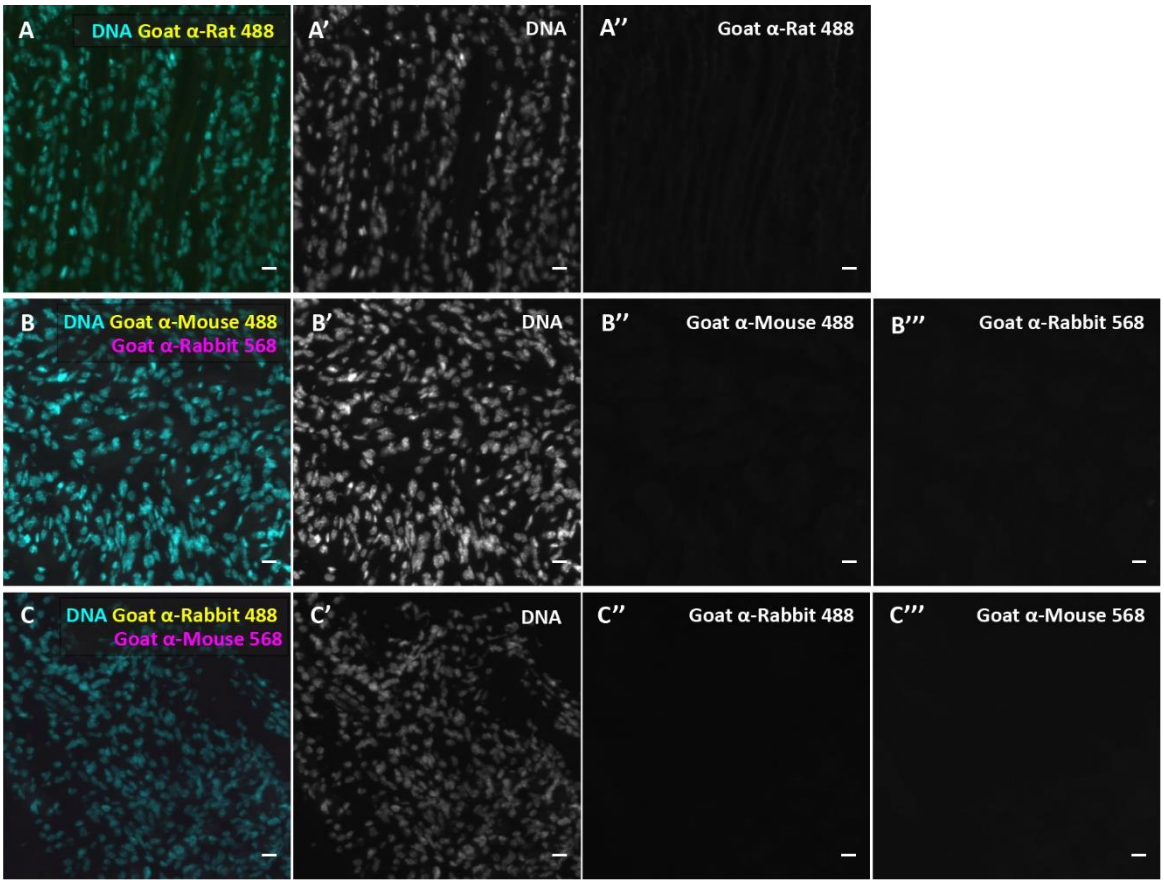

Figure S. 1 – Negative controls of the secondary antibodies. Immunostaining with secondary antibody Goat α-Rat Alexa 488 (**A**, yellow; **A''**, grayscale), Goat α-Mouse Alexa 488 (**B**, yellow; **B''**, grayscale), Goat α-Rabbit Alexa 568 (**B**, magenta; **B'''**, grayscale), Goat α-Rabbit Alexa 488 (**C**, yellow; **C''**, grayscale) Goat α-Mouse Alexa 568 (**C**, magenta; **C'''**, grayscale) and DNA (**A**, **B**, **C**, cyan; **A'**, **B'**, **C'**, grayscale). The color image (**A**, **B**, **C**) is a merge of the respective grayscale channels. Scale bars: 15µm.

Annex III – Western Blot

Table S. 2 – Western Blot band intensity bands values and ratio.

WB Quantification							
NT	**LAMA2 6%**	**LN 6%**	**COL I 8%**	**COL VI 8%**	**FN 8%**	**LANE 6% (Ponceau Red)**	**LANE 8% (Ponceau Red)**
WT1	**15.579.856**	**49.325.851**	**3.418.811**	**4.849.104**	**10.611.326**	**34.850.630**	**40.583.496**
WT2	**18.194.061**	**40.213.245**	**2.547.276**	**3.625.246**	**11.609.912**	**38.612.709**	**40.615.851**
WT3	**21.566.688**	**36.123.274**	**3.244.225**	**5.950.510**	**17.770.167**	**44.626.591**	**47.597.940**
dy$^{W-/-}$*1*	**9.835.099**	**11.425.271**	**4.138.548**	**5.379.167**	**4.988.669**	**28.423.680**	**19.614.362**
dy$^{W-/-}$*2*	**7.235.350**	**10.349.200**	**4.212.619**	**4.731.711**	**5.460.912**	**24.371.571**	**22.421.434**
dy$^{W-/-}$*3*	**4.558.250**	**10.526.685**	**3.995.326**	**5.998.832**	**4.180.205**	**28.174.697**	**20.446.132**
Protein/Lane Profile ratio							
WT1	**0,44704661**	**1,415350339**	**0,084241412**	**1,418359775**	**0,261468997**	**34.850.630**	**40.583.496**
WT2	**0,471193591**	**1,041451016**	**0,062716303**	**1,423185395**	**0,285846824**	**38.612.709**	**40.615.851**
WT3	**0,483269896**	**0,809456272**	**0,068158937**	**1,83418536**	**0,373338993**	**44.626.591**	**47.597.940**
dy$^{W-/-}$*1*	**0,346017792**	**0,401963117**	**0,2109958**	**1,299771562**	**0,254337561**	**28.423.680**	**19.614.362**
dy$^{W-/-}$*2*	**0,296876635**	**0,424642301**	**0,187883567**	**1,123223107**	**0,24355766**	**24.371.571**	**22.421.434**
dy$^{W-/-}$*3*	**0,161785236**	**0,373621942**	**0,195407425**	**1,501462459**	**0,204449673**	**28.174.697**	**20.446.132**

Note: LAMA2 means laminin α2, LN means pan-Laminin, COL I means collagen I, COL VI means collagen VI and FN means fibronectin.

Table S. 3 – ANOVA results using genotype as the criterion

Protein	Predictor	*df*	Sum of Squares	Mean Square	F-value	p-value
Laminin α2	Genotype (WTx*dy*$^{W-/-}$)	1	0.059	0.059	12.576	0.023 *
Pan-laminin		1	0.711	0.711	15.119	0.017 *
Collagen I		1	0.0239	0.023	181.37	0.0001 ***
Collagen VI		1	0.094	0.094	2.027	0.227
Fibronectin		1	0.007	0.007	3.828	0.122

Note: *df* means degrees of freedom. * indicates p<0.05. ***indicates p<0.0001.

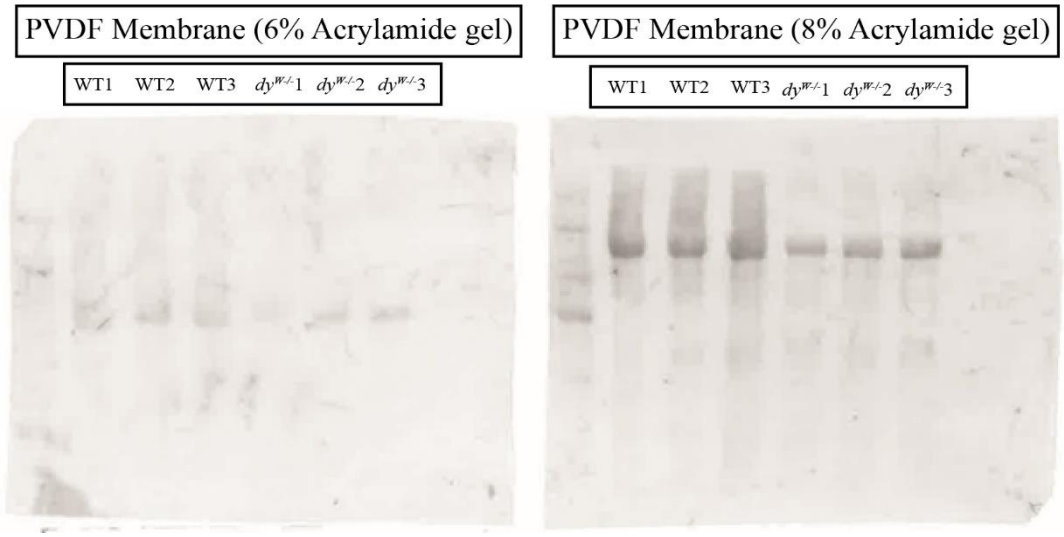

Figure S. 2 – Ponceau Red staining profile in the PVDF membranes.

Annex IV – Cell Counting

Table S. 4 – Cell counting of the recellularized matrices of both genotypes.

8 Days									
WT1	**WT2**	**WT3**	**WT4**	**WT5**	**WT6**	**WT7**	***dy*$^{W-/-}$1**	***dy*$^{W-/-}$2**	***dy*$^{W-/-}$3**
211	223	60	195	184	277	218	183	185	166
73	164	201	264	212	299	258	75	136	189
MV	260	164	MV	233	200	MV	106	115	131

Note: MV means missing value.

Table S. 5 – ANOVA analysis of the number of cells per genotype

	Predictor	Estimate Standard Deviation	Error	*df*	T-value	p-value
Number of cells	(Intercept) (*dy*$^{W-/-}$)	142.889	22.504	6.851	6.349	0.0004***
	WT	62.334	27.327	7.243	2.281	0.055

Note: *df* means degrees of freedom. ***indicates p<0.0001.